INL/EXT-18-52306-Revision-0

Continuation Report: Creep-fatigue Behavior and Damage Accumulation of a Candidate Structural Material for Concentrating Solar Thermal Receiver

Michael D McMurtrey, Mark Messner, Bipul Barua

December 2018

The INL is a U.S. Department of Energy National Laboratory
operated by Battelle Energy Alliance

Idaho National Laboratory

INL/EXT-18-52306-Revision-0

Continuation Report: Creep-fatigue Behavior and Damage Accumulation of a Candidate Structural Material for Concentrating Solar Thermal Receiver

Michael D McMurtrey, Mark Messner, Bipul Barua

December 2018

Idaho National Laboratory
Idaho Falls, Idaho 83415

http://www.inl.gov

Prepared for the
U.S. Department of Energy
Office of Energy Efficiency and Renewable Energy
Under DOE Idaho Operations Office
Contract DE-AC07-05ID14517

Continuation Report

Project Title:	Creep-fatigue Behavior and Damage Accumulation of a Candidate Structural Material for Concentrating Solar Thermal Receiver
Project Period:	2/01/18 – 1/31/20
Budget Period:	2/01/18 – 10/31/18
Submission Date:	12/1/18
Recipient:	Idaho National Laboratory
Address:	2525 Fremont Ave Idaho Falls, ID 83415
Website (if available)	www.inl.gov
Award Number:	33872
Project Team:	Idaho National Laboratory Argonne National Laboratory
Principal Investigator:	Michael McMurtrey, Materials Scientist Phone: 208 526-2327 Email: michael.mcmurtrey@inl.gov
Business Contact:	Gabriel Ilevbare, Materials Science and Engineering Manager Phone: 208 526-3735 Email: gabriel.ilevbare@inl.gov
HQ Tech Manager:	Mark Lausten
HQ Project Officer:	Christine Bing
GO Grant Specialist:	GS name
GO Contracting Officer:	CO name

Executive Summary

At the start of this phase, six alloys were determined to be candidate materials for the concentrating solar power (CSP) thermal receiver: Alloys 617, 625, 740H, 230, 282 and Alloy X. From these, Alloys 740H and 282 were determined to be the most suitable, with both alloys exhibiting similar high temperature strength properties. Alloy 740H was selected due to its ease to work with (simpler heat treatments and welding procedures) and a larger database of existing data.

Fatigue testing was started in this phase, with four fatigue tests having been completed, with additional fatigue testing planned, as well as tensile, creep and creep-fatigue tests starting in the next phase. Two fatigue tests performed at 850 °C and were completed in significantly fewer cycles than the two tests performed at 750 °C. Metallography was performed on the fatigued specimens to examine crack path and surrounding microstructure. These preliminary results suggest a significant drop in strength at elevated temperatures above 750 °C, however, more test results will be needed prior to setting design limits.

Several potential model high temperature design methods were evaluated that could form the basis of our final recommended creep-fatigue design method for Alloy 740H. To do this we expanded on the receiver finite element model to develop a model representative of a potential Gen 3 design using KCl-MgCl2 salt coolant and operating with a salt inlet temperature of 550°C and salt outlet temperature of 720°C. Using the temperature fields from the model thermohydraulic analysis we determined the design life of the reference receiver assuming it was constructed from 740H seamless tubing and assuming high temperature design properties for 740H from literature data and, where required, naïve extrapolation. As experimental data is generated, these tentative design parameters will be updated to match the actual performance of 740H in elevated temperature service.

The results of this design study are a rank ordering of potential design methods for two criteria: ease of use and design margin. The end goal of this project is to develop a creep-fatigue design method with adequate, but not over conservative, design margin that is straightforward to execute.

Our receiver model is based on the preliminary design provided to DOE by Solar Reserve. Our analysis indicates a peak metal temperature of around 840° C for this design (comparable to Solar Reserve's analysis, which shows a peak metal temperature of around 830° C). The Solar Reserve tube thickness is too thin to sustain creep-fatigue loading at this temperature. This means that the current trial design is not well-suited for evaluating different design methodologies, as we predict it will have a very short design life. We suggest that we modify our reference design with input from DOE in order to lower the maximum metal temperature to less than 800° C. We can then repeat these analyses and give a more meaningful comparison of different design methods before making a final selection.

Table of Contents

Executive Summary 2
Background 4
Introduction 6
Project Results and Discussion 7
Task 1 7
Task 2 17
Conclusions 47
Budget and Schedule 47
Path Forward 47
References 48

Background

Concentrating solar power (CSP) thermal receivers are heated by reflecting sunlight off an array of mirrors onto a central point (the receiver). The nature of this heating is such that the receiver temperature is directly tied to the amount of sunlight, causing large temperature drops during cloud cover and after the sun has set. Creep-fatigue deformation is an important consideration for a thermal receiver of a CSP system due to the constant static stress or pressure, diurnal cycling, and elevated service temperatures required for efficient operation [1-3]. An assessment of a solar thermal receiver design must include quantification of the expected creep-fatigue damage to evaluate whether a candidate material is capable of meeting cost and lifetime goals [2, 3]. One such receiver design has been proposed by Solar Reserve, and is used for a basis in this work [4]. Experimentally creep-fatigue testing, which introduces a strain-controlled hold time in a fatigue cycle, is often used to approximate the intermittent cycling during high temperature service. Creep-fatigue deformation is known to accelerate failure relative to that expected from isolated creep and fatigue cycling as a result of interaction between the deformation modes [5-7].

A component of the overall CSP technology meeting cost goals is the material of construction for the receiver and the receiver's ability to meet lifetime requirements, in this case 30 years or 10,000 cycles [2, 3]. Candidate materials for a thermal receiver are commercial nickel-base alloys, Inconel 625, Inconel 740H, Haynes 230, and Haynes 282 [1], and are relatively expensive in comparison to stainless steels. These alloys are predominantly strengthened by solid solution strengthening and have appreciable amounts of Cr [8, 9]. While many of the physical and mechanical properties such as the creep and low cycle fatigue are readily available [8, 9], the creep-fatigue properties are not.

Creep-fatigue data is critical for design as it is the basis of the creep-fatigue interaction diagram, otherwise known as a D-diagram, constructed using a linear damage summation of the individual creep and fatigue terms, such as in the case of the American Society of Mechanical Engineers (ASME) Boiler and Pressure Vessel Code Section III, Division 5 (Subection HB, Subpart B for Class A components at elevated temperatures) [10]. The interaction is accounted for empirically by summing, then plotting, the two types of damage. The interaction is represented by bilinear curves, which vary for different materials, forming the damage envelopes within which the calculated damage for a design must fall. A reproduction from [11] of the creep-fatigue interaction diagram for the ASME Section III Division 5 materials [10] is shown in Figure 1(a). While these rules may be more conservative than necessary for a CSP application [3, 12], a linear summation damage assessment is typically utilized for creep-fatigue [13] and an accurate assessment of a CSP thermal receiver material will likely require a valid D-diagram to assess preliminary designs.

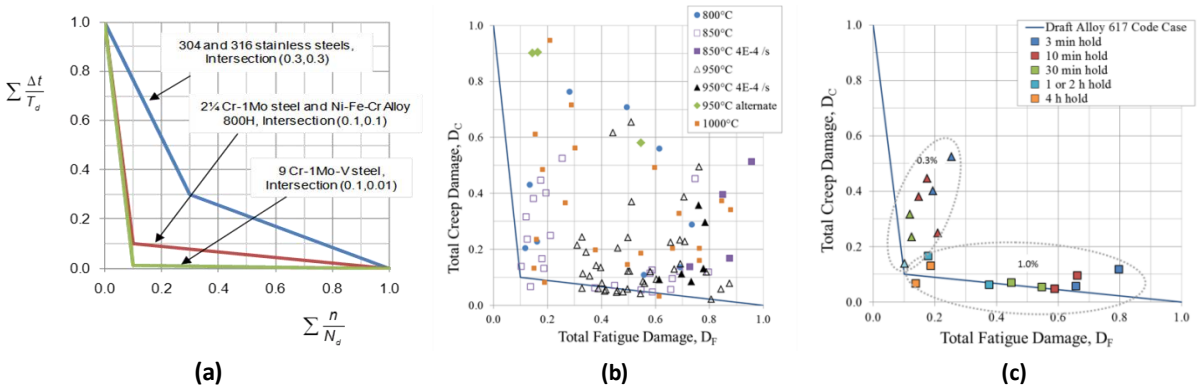

Figure 1 – (a) Creep-fatigue interaction diagram reproduced [11] from ASME Section III, Division 5, Subsection HB, Subpart B [10]. Nickel-base alloy, Alloy 617, creep-fatigue interaction diagram [11] developed from (b) all available data points in references [14, 15, 17, 18] and (c) with only data generated at 850 °C for the two strain ranges, 0.3% total strain and 1.0% total strain.

There are three manuscripts available that detail the modeling of the expected creep-fatigue damage in a solar thermal receiver [2, 3, 12]. Ortega et al. [3] have modeled a s-CO2 tubular thermal receiver design using Inconel 625 and considered the lifetime cycling requirement as 10,000 diurnal cycles (30 years), a 9 to 10 hour day from [12], a maximum temperature of 800 °C, and pressure of 30 MPa. The creep-fatigue analysis [3] is done according to simplified design rules based on the nuclear Code and assumes no creep-fatigue interaction, i.e. a line passing through the point 0.5, 0.5 on the creep-fatigue interaction diagram. The basis for the latter assumption is not clear since the Special Metals technical data sheet for Inconel 625 [8] is referenced but does not provide creep-fatigue property data or a damage parameter. This modeling to assess feasibility of the receiver resulted in the creep damage equaling approximately 0.9 and the fatigue damage approximately 0.1, thus outside of the design envelop for all Section III, Division 5 materials shown in Figure 1(a). The most similar alloy, Alloy 800H, in Figure 1(a) has an intersection point of 0.1, 0.1.

Similarly, Neises et al. [12] considered Haynes 230 for a tubular receiver operating at 650 °C and again assumed no creep-fatigue interaction (a D value of 1) based upon the work of Chen et al. [13]. The D-diagram in reference [13] was constructed based upon a very limited number of creep-fatigue data points. Chen et al. acknowledge that for a similar nickel-base alloy, Alloy 617, also investigated, many of these still very limited data points fall to the left of a line with an intersection point of 0.5, 0.5 [13]. This assumption of no creep-fatigue interaction, instead of accounting for one through a lower intersection point, leads to the conclusions that the design/material is capable of the 30 year lifetime with an accumulated damage of 0.9962. Although considering much higher temperatures, Fork et al. investigated an Alloy 617 solar thermal receiver for an air Brayton cycle and found the operating conditions would be challenging and likely not feasible at 980 °C but may at 870 °C [2].

The assumptions made regarding the creep-fatigue design analyses for s-CO2 CSP thermal receiver designs may not be sufficiently conservative thus it is likely they have a

much lower creep-fatigue life than calculated. Therefore, a better understanding of the creep-fatigue behavior of a candidate material and the associated design rules should be developed. An accurate description of the creep-fatigue behavior, not available for the four mentioned candidate materials [1], is important for assessment of preliminary designs.

Recently, the Advanced Reactor Technologies program, funded through the Department of Energy (DOE) Office of Nuclear Energy, supported the ASME Code qualification of Alloy 617 into Section III, Division 5 Subsection HB, Subpart B [11]. Alloy 617 creep-fatigue behavior is likely similar to CSP receiver candidate structural materials and an extensive amount of data at 850 and 950 °C [14, 15, 17, 18] has been compiled and a creep-fatigue interaction diagram constructed [11], as shown in Figure 1(b). The results support those of the initial draft ASME Code Case for Alloy 617 recommending a D-diagram intersection point of 0.1, 0.1 [16]. As shown in Figure 1(c), at the lower temperature, 850 °C, many of the longer hold durations showed the accumulation of significant creep damage and reside near the 0.1, 0.1 bi-linear curve intersection. The lower strain range condition and the longer hold time durations, more applicable to thermal receivers, were not investigated by Chen et al [13] in the development of their published Haynes 230 creep-fatigue interaction diagram. The latter is important because of the lack of creep-fatigue saturation at long hold times at 850 °C, i.e. increasing hold time duration results in decreasing cycle life for all investigated hold times [18]. This recent work on Alloy 617 suggests the need for a more thorough investigation of the creep-fatigue behavior of candidate receiver materials at the expected service temperatures of 700 to 800 °C and the associated creep-fatigue design rules.

Introduction

Creep-fatigue deformation is an important consideration for a thermal receiver of a gas phase (GP) Concentrating Solar Power (CSP) system due to the constant static stress or pressure, diurnal thermal cycling, and elevated service temperatures required for efficient operation. An accurate description of the creep-fatigue behavior, not available for five of the six candidate materials, is important for assessment of preliminary designs. This project seeks to provide a detailed analysis of the creep-fatigue behavior and damage accumulation of a candidate structural material for a CSP solar thermal receiver to address a critical knowledge barrier for receiver design in the GP pathway concept identified in the CSP Gen3 Demonstration Roadmap. This effort includes the development of rules for the design of solar receiver components against high temperature creep-fatigue and ratcheting failure modes. The ASME Code rules for high temperature nuclear components will form the basis of the method but adjustments will be made to reflect the generally shorter, diurnal operating cycles of thermal receivers and the relative consequences of failure, comparing nuclear to solar components.

The project has been divided into three tasks. Task 1, Creep-Fatigue Testing and Metallographic analysis, focuses on the low cycle fatigue and creep-fatigue testing. Fatigue testing will be performed mostly between temperatures of 750-850°C, as well as creep-fatigue testing with hold times in the range of 0.5 to 4 hours and multiple strain ranges of a candidate receiver alloy. Subsequent data and metallurgical analysis will be performed on the tested specimens which will be used to provide data to Task 2. Task

2, Analysis of Design Methodology, which will analyze the design rules for solar thermal receivers and the experimental test data to develop a design method for ratcheting and creep-fatigue for a single temperature. An evaluation of appropriate modifications to current design rules that is applicable for solar receiver components from which the results will be summarized into a set of proposed design rules. Task 3 originally was the Assessment of Environmental Interaction, however, based on some early feedback from industrial partners, the focus of this task has been shifted to do some preliminary work looking at different forms of materials (such as sheet).

There are several milestones associated with each task. For Task 1, the work in this phase has focused on Milestone 1: Alloy Selection, which was completed in this phase (Alloy 740H was selected), and Milestone 2:Completetion of Fatigue and Preliminary Creep-Fatigue Testing – Procurement of material and machining of specimens for mechanical testing has been completed and preliminary testing has started. For Task 2, milestones 1 and 2 have been completed (Receiver design rules were aligned with industry practice and available creep data was compiled and analyzed). The goals of this phase have been to evaluate several potential model high temperature design methods that could form the basis of our recommended creep-fatigue design method for Alloy 740H. The receiver finite element model described previously will be expanded on to develop a model representative of a potential Gen 3 design using KCl-MgCl2 salt coolant and operating with a salt inlet temperature of 550°C and salt outlet temperature of 720°C. As experimental data is generated, these tentative design parameters will be updated to match the actual performance of 740H in elevated temperature service. Task 3 is a second phase task, goals have shifted to examine material forms beyond the originally planned plate. Task 3 begins in year 2, however, this material was procured in this phase to ensure that specimens are ready for testing when the task begins.

Project Results and Discussion

Task 1

Alloy selection

Alloy Selection was based on a number of factors, including various mechanical properties (strength at room temperature (RT), 750°C, 850°C; weldability and weld strength; complexity of the required heat treatments and available creep and fatigue data). Each criteria was given a weighting factor that reflected its relative importance in the alloy selection process. High temperature strength was given the highest weight fact, and room temperature strength the lowest. The resulting scores are shown in Table 1.

		Alloy 625		Alloy 617		Alloy 230		Alloy X		Alloy 740H		Alloy 282	
Criteria	Weighting Factor	Score	Rating	Score	Rating	Score	Rating	Score	Rating	Score	Rating	Score	Rating
Strength at RT	0.07	2	0.14	1	0.07	3	0.21	2	0.14	3	0.21	3	0.21
Strength at 750 °C	0.25	2	0.5	2	0.5	2	0.5	1	0.25	3	0.75	3	0.75
Strength at 800 °C	0.25	2	0.5	2	0.5	2	0.5	2	0.5	2	0.5	2	0.5
Weld strength reduction factor	0.18	3	0.54	3	0.54	2	0.36		0	2	0.36	4	0.72
Complexity of aging treatment	0.12	3	0.36	4	0.48	4	0.48	4	0.48	3	0.36	2	0.24
Alloy weldability	0.13	3	0.39	3	0.39	3	0.39	3	0.39	3	0.39	1	0.13
TOTAL	1		2.43		2.48		2.44		1.76		2.57		2.55

Table 1. Alloy scores for determining suitability CSP thermal receiver alloy.

Alloys 740H and 282 scored the highest, with nearly identical scores. Preliminary design curves for stress allowables for a 100,000 hour rupture life indicate that the allowable stresses for Alloy 740H and 282 will also be similar (Figure 2). Given the similarities in desirable properties, Alloy 740H was selected due to the slightly higher selection score (Table 1) and the larger existing database for creep and fatigue measurements.

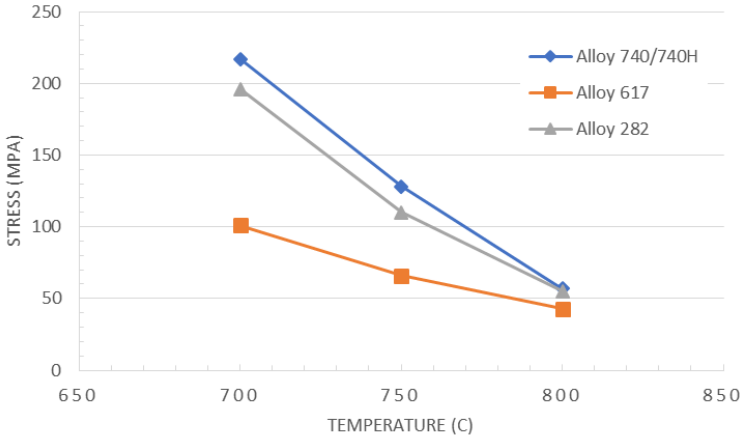

Figure 2. Preliminary allowable stresses calculated for a 100,000 hour life for Alloys 740H and 282 (with 617 as a reference).

Fatigue testing

1.5" plate was ordered from Special Metals for use in the project. To help facilitate an earlier start to testing, some existing 1.5" plate at INL was borrowed from a separate project in order to machine specimens while awaiting the newly ordered plate. Fatigue tests were performed at both 750°C and 850°C, with two replicates at each test. The test was controlled to a total strain range ($\Delta\varepsilon_t$) of 1% (±0.5%), with a 0.001 /sec strain rate was used for all testing. No hold time (t_h) was used for fatigue testing. This is recorded in the results as 0 to differentiate the fatigue tests from the creep fatigue tests which will have a $t_h > 0$. The peak tensile and compressive stresses are shown per cycle in Figure 3.

During the fatigue test, a reference point is chosen and the peak stress is recorded. The test is terminated when a set drop in peak load has occurred. This termination is to prevent specimen rupture, which can be damaging to the specimen and the equipment. For the first test performed at 850°, the reference point was chosen to be at 500 cycles. The test, however, finished prior to reaching 500 cycles, resulting in this specimen rupturing. The reference point for the first test performed at 750°C was chosen more conservatively, between 150 and 200 cycles, however, due to the significant cyclic softening of this material, the end of test was triggered before significant cracking of the specimen. As knowledge of the behavior of the material was gained, the termination conditions for the replicate tests were chosen in such a way as to ensure termination of the test occurred at the desired point.

In Figure 3, after an initial sharp increase in stress vs cycle, the values level off and the change in peak stress is linear with cycle count. After some time, the tests deviate from linearity and begin to decrease more rapidly. This deviation from linearity is considered to be the onset of cracking (N_0). Fatigue life is determined by a percent drop in stress from the onset of cracking. In this work, a 25% drop in life was used to determine fatigue life (N_{25}). The tests performed at 850°C were found to have a fatigue life of ~400 cycles, whereas the 750°C tests exhibited a much higher fatigue life, around 1800 cycles.

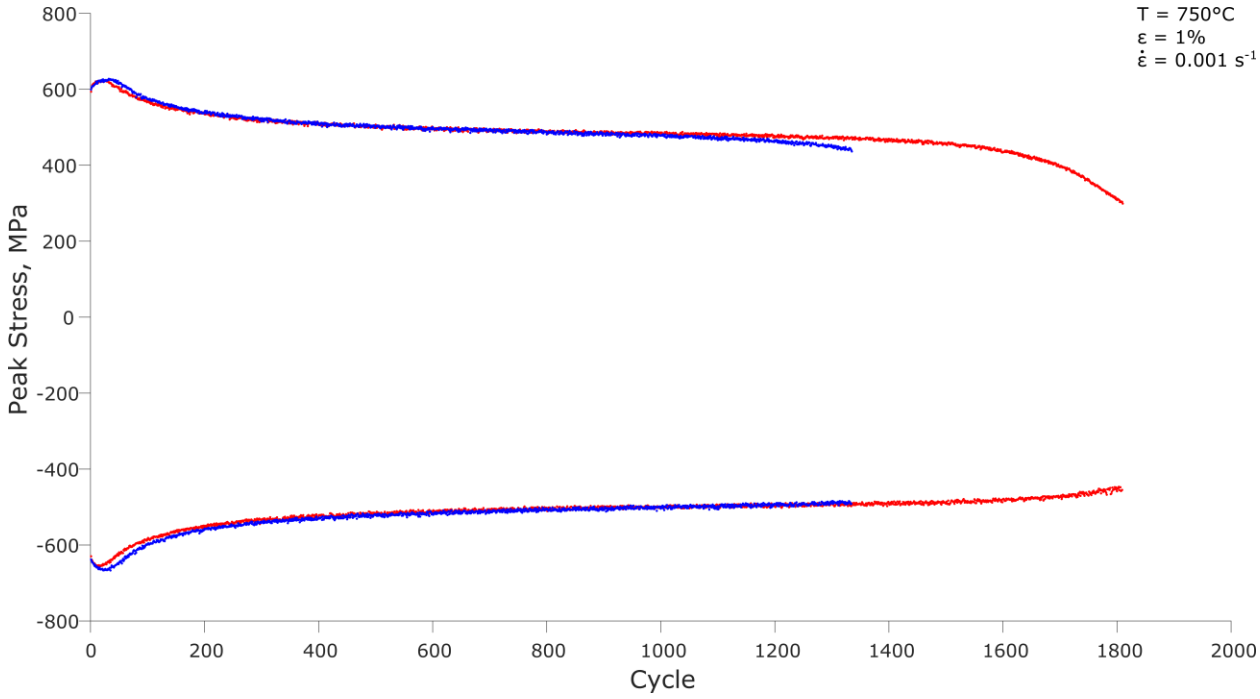

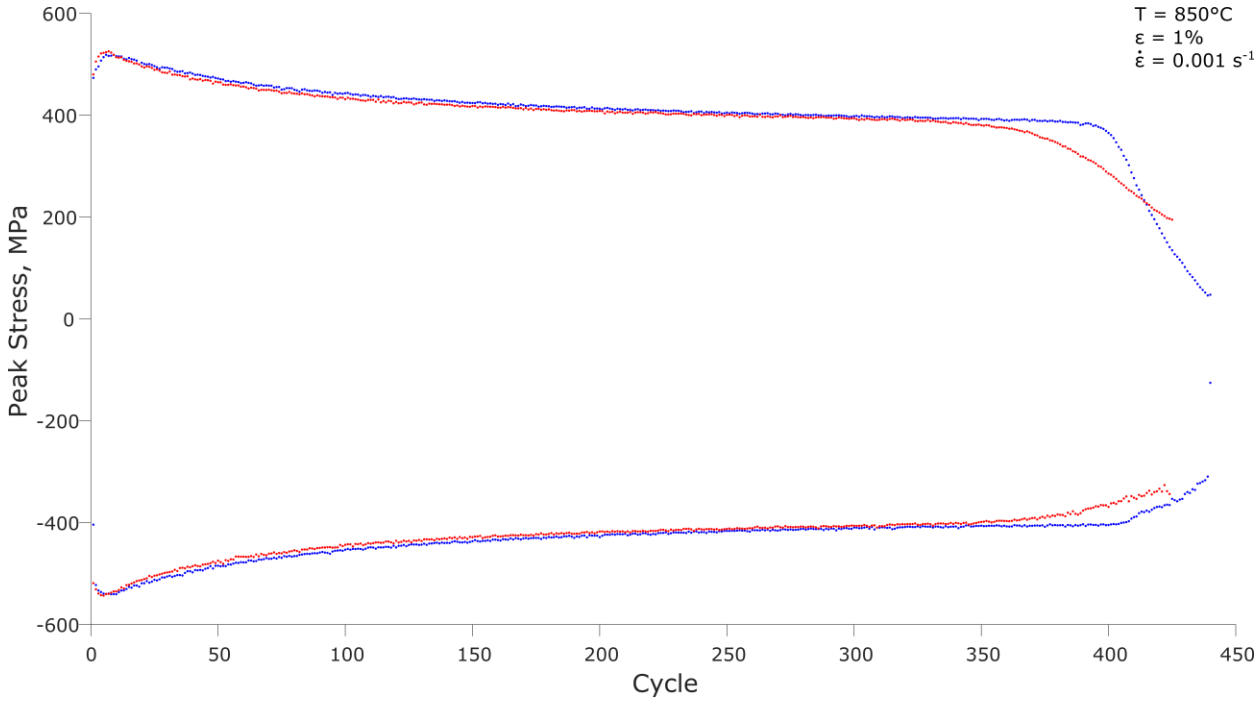

Figure 3. Peak stress vs. cycle count for specimens tested at 750°C (top) and at 850°C (bottom).

In addition to the peak stress vs. cycle, the hysteresis loops, showing the stress vs strain for a given cycle, are shown for the beginning of the test (cycle 10) and the mid-cycle (half of the fatigue life). These are shown in Figure 4 and 5. Hysteresis loops help highlight the material behavior during testing, and can be used to find peak stresses (σ_{max} and σ_{min} for the peak tensile and compressive stresses, respectively) for a given cycle. The width of the hysteresis loop is related to the plastic deformation occurring during the cycle, with the earlier loops being narrower, and midlife loops being wider, due to the cyclic softening occurring during testing. The results of these four fatigue tests are summarized in Table 2.

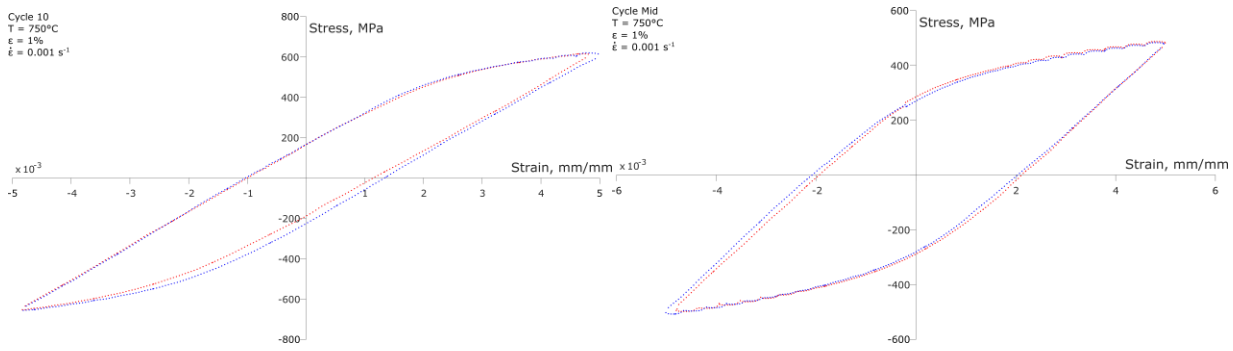

Figure 4. Hysteresis loops for one of the specimens tests at 750°C, showing early life (left) and midlife (right).

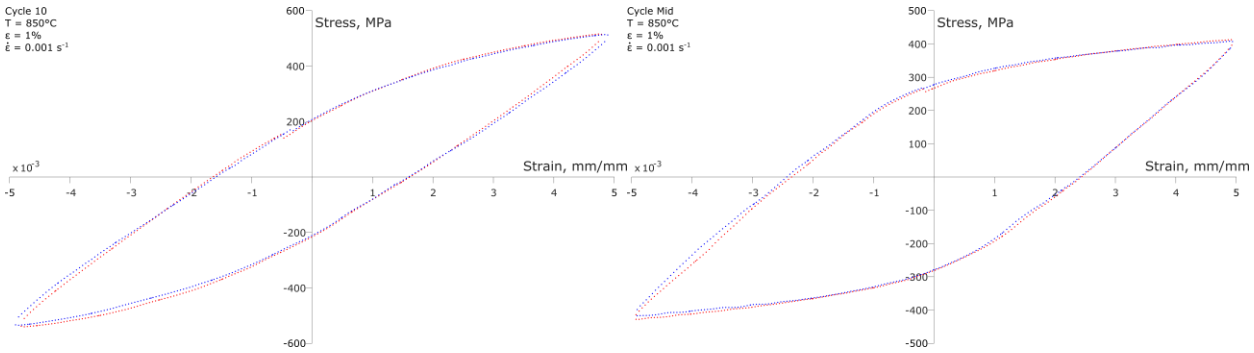

Figure 5. Hysteresis loops for one of the specimens tests at 850°C, showing early life (left) and midlife (right).

Specimen ID	Temp.	Strain Rate	t_h	$\Delta\varepsilon_t$	At Cycle 10		Midlife				
					σ_{max}	σ_{min}	cycle used	σ_{max}	σ_{min}	Cycles to Initiation	Cycles to Failure
	(^oC)	(/s)	(min)	(%)	(MPa)	(MPa)	($N_{25}/2$)	(MPa)	(MPa)	(N_0)	(N_{25})
740H-BF1	850	0.001	0	1.0	516	-540	200	413	-428	398	409
740H-BF2	750	0.001	0	1.0	620	-656	900	483	-508	-	-
740H-BF3	750	0.001	0	1.0	616	-653	900	487	-498	1541	1767
740H-BF4.	850	0.001	0	1.0	514	-535	200	408	-417	370	402

Table 2. Summary of fatigue testing performed in Q3.

Metallography

Following the fatigue testing, the gauge sections of the specimens were imaged in a Keyence Optical Microscope to show the primary and secondary cracking (Figures 6 and 7). In general, all specimens exhibited a large primary crack in the center region of the gauge section, with only a few other smaller secondary cracks. The surface is also decorated with micro-cracks which did not propagate any significant distance into the gauge section.

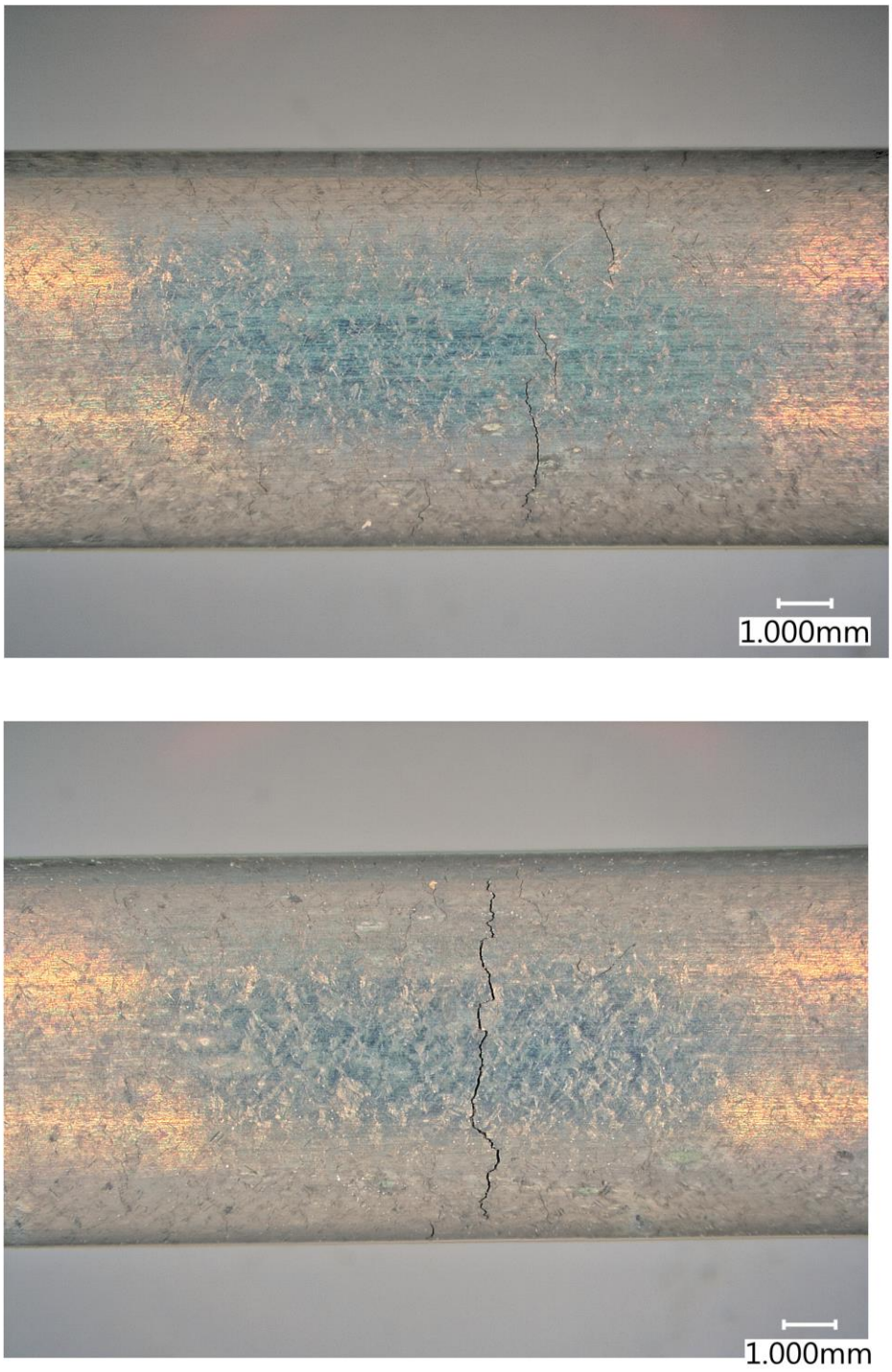

Figure 6. Gauge sections of the two specimens tested at 750°C.

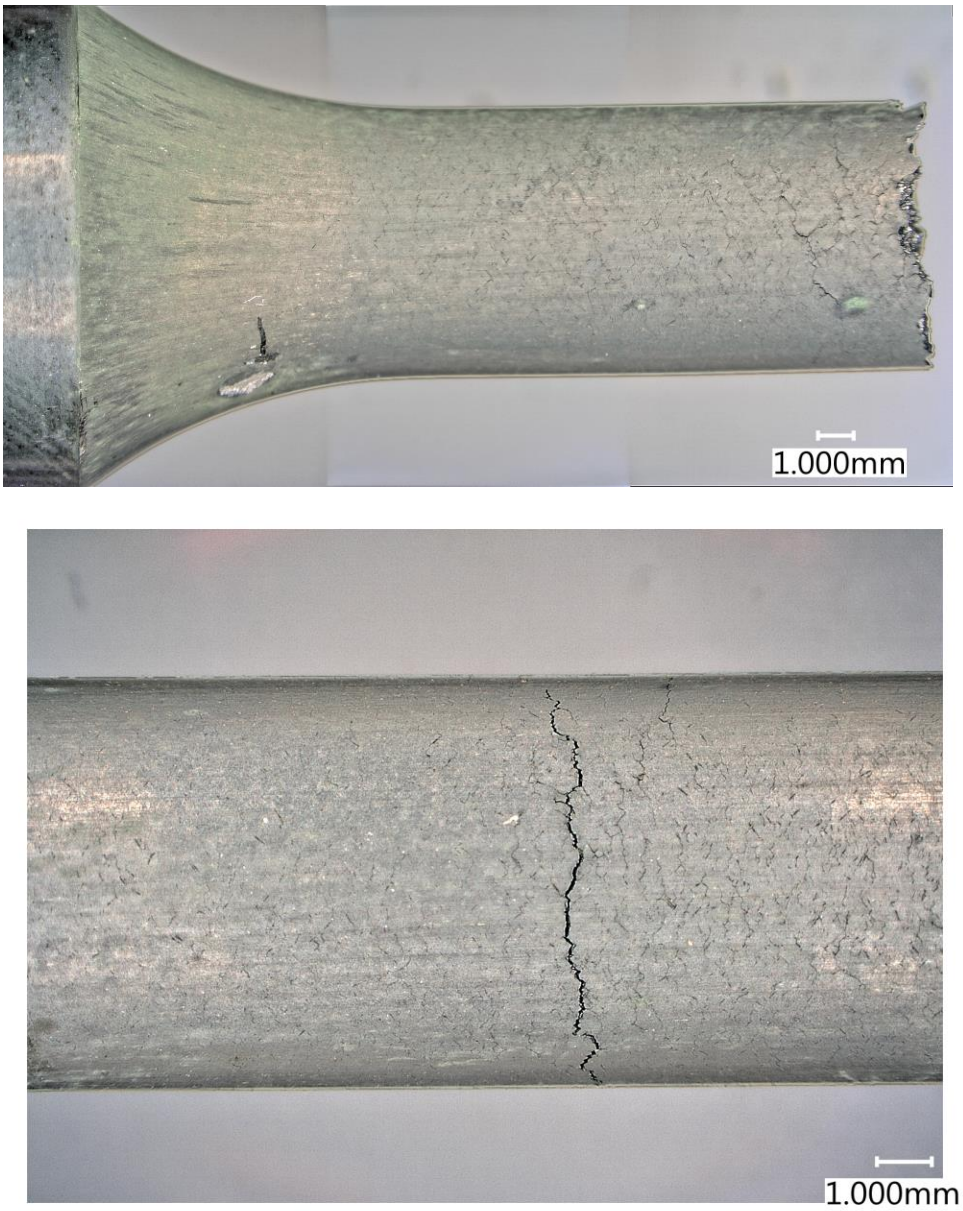

Figure 7. Gauge sections of the two specimens tested at 850°C.

Specimens were cross sectioned at the gauge such as to cut the primary (largest) crack in half. The cross sections were polished and etched with an oxalic acid and a 2.2V applied potential for 12 seconds to reveal the grain microstructure, and imaged in the Keyence Microscope. Figures 8 and 9 show the cross sections of the primary crack. The images show cracks that contain mix mode (both intergranular and transgranular) cracking. The specimens tested at 750°C appear to have a larger degree of transgranular cracking than the specimens tested at 850°C, however, there is not enough data with these specimens to indicate if there is actually a change in crack behavior at the two different temperatures. A change from transgranular to intergranular could suggest a significant change in microstructure, such as precipitation

at the grain boundary, which could be linked to the sudden drop in fatigue life at higher temperatures. This will be explored in greater detail in subsequent work.

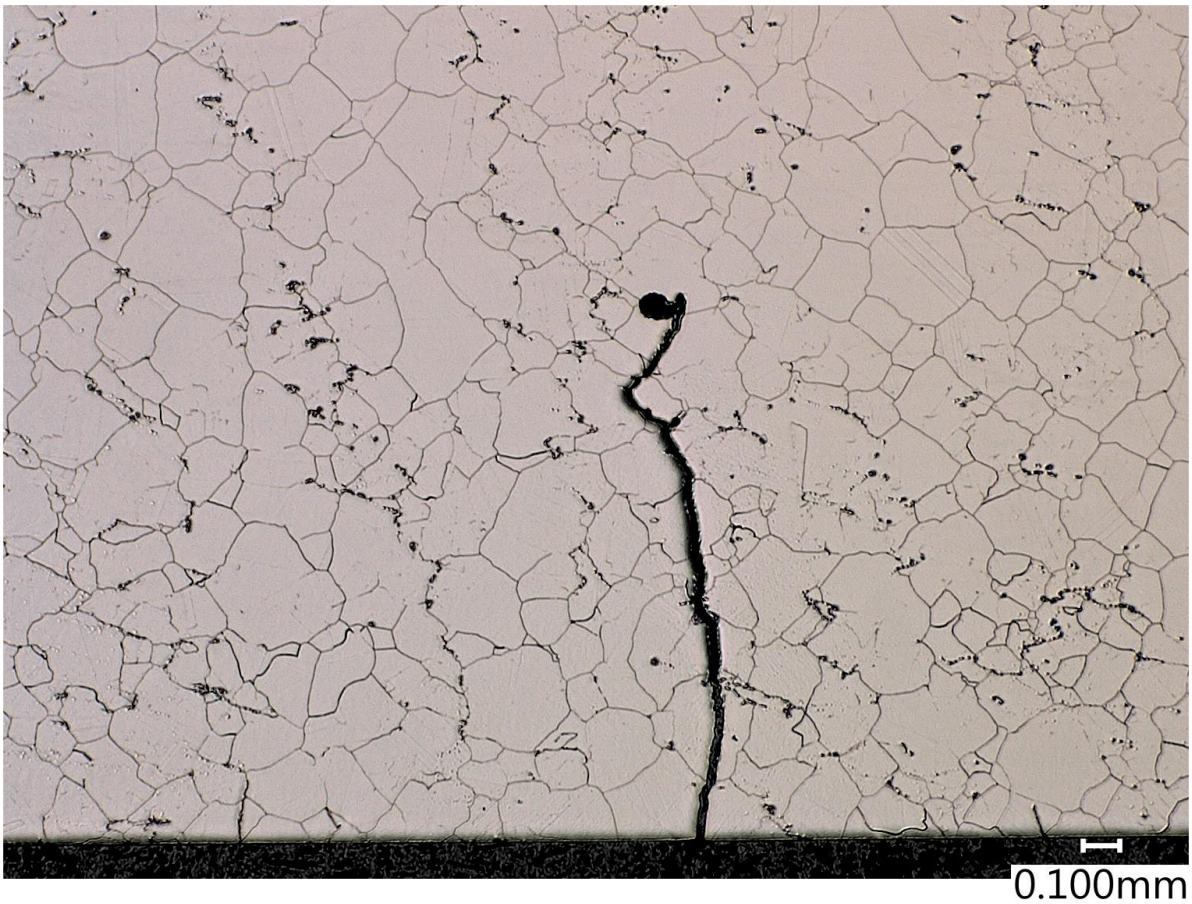

Figure 8. Cross sections of primary cracks in the two specimens tested at 750°C. The upper image is from the specimen that ended prematurely and did not progress to failure (N_{25}).


0.100mm

Figure 9. Cross sections of the primary cracks from the specimens tested at 850°C. Upper image shows the specimen that was not stopped in time and proceeded to rupture.

Task 2

Preliminary design rule recommendations

This report describes several potential high temperature creep-fatigue and ratcheting design processes. It also quantifies the effect of several different design margins applied to the creep-fatigue design data (creep rupture stresses and fatigue diagrams). Our receiver model is based on the preliminary design provided to DOE by Solar Reserve [4]. Based off this preliminary analysis we are targeting a modified version of the Section III, Division 5 design by inelastic analysis rules. Given analysis results these rules are simple to execute and provide the most accurate, and also longest, design life for a given component. The challenge with design by inelastic analysis is that the analysis step is quite complicated. The method requires a complete inelastic model describing the material response. Developing such a model is a research program in itself. Additionally, the Section III, Division 5 rules require a designer to simulate the full time-history of the component. This could be a significant computational challenge.

We propose to keep the inelastic analysis acceptance criteria while modifying the analysis method to use a simplified elastic, perfectly plastic, power law creep material model. We would provide material constants describing this response for Alloy 740H. This constitutive model is history independent, meaning that a designer could simulate design load cycles separately and combine the effects together, much like how current simplified high temperature design methods work. Additionally, we would base the design off the steady state, cyclic plasticity solution to avoid requiring the designer to follow the full load history of their component. This proposed method could combine simple analysis and simple acceptance criteria while still retaining accurate, not over-conservative design predictions.

Alloy 740H design rules and supporting analysis

Preliminary design data

In order to evaluate competing design methods material properties and design data are needed. We have identified a database of relevant experimental data in past reports. However, the existing literature data is insufficient to develop a full creep-fatigue design method, hence this project and the planned experiments. While waiting for the 740H data, a completely notional set of design allowables were developed, reasonably representative for 740H, in order to evaluate some trial design methods. Some of these design data will remain more or less the same in the final report (for example, the rupture stress correlations) but most of it will change, potentially drastically, as the experimental data becomes available.

Young's modulus

These values are from the material datasheet [19], extrapolated to high temperatures where required.

Temperature (°C)	Modulus (GPa)
20	221
100	218
200	212
300	206
400	200
500	193
600	186
700	178
800	169
900	160
950	155

Table 3. Design Young's modulus.

Poisson's ratio

Based on the ASME Section II values we elect to use a constant value of 0.31.

Coefficient of thermal expansion

These values are from the material datasheet [19], extrapolated to high temperatures where required.

Temperature (°C)	Mean CTE (μm/mm/°C)	Instantaneous CTE (μm/mm/°C)
20		11.69
100	12.38	12.97
200	13.04	13.97
300	13.5	14.75
400	13.93	15.38
500	14.27	15.67
600	14.57	16.64
700	15.03	18.86
800	15.72	22.11
900	16.41	26.38
950	16.76	28.9

Table 4. Design coefficients of thermal expansion.

Thermal conductivity

These values are from the material datasheet [19], extrapolated to high temperatures where required.

Temperature (°C)	Conductivity (W/(m °C))
20	10.2
100	11.7
200	13
300	14.5
400	15.7
500	17.1
600	18.4
700	20.2
800	22.1
900	23.8
1000	25.4

Table 5. Design values of thermal conductivity.

Specific heat

These values are from the material datasheet [19], extrapolated to higher temperatures where required.

Temperature (°C)	Specific heat (J/(kg °C))
20	449
100	476
200	489
300	496
400	503
500	513
600	519
700	542
800	573
900	635
1000	656

Table 6. Design values of specific heat

Yield strength

This data comes from the 740H ASME Code Case [20]. To bound material variation the ASME Code scales the average material response by the ratio of the specified minimum yield stress (620 MPa for 740H) to the average yield stress at room temperature. Values were interpolated and extrapolated as required.

Temperature (°C)	S_y (MPa)
40	621
100	594
150	577
200	562
250	548
300	538
350	531
400	529
450	529
500	529
550	529
600	529
650	529
700	529
750	508
800	463
850	418
900	373

Table 7. Design values of yield strength (S_y).

Ultimate tensile strength

This data comes from the ASME Code Case [20]. As with the yield strength, the ASME Code calculates a lower bound property to account for material variation by scaling the average strength to match the minimum specified ultimate tensile strength (1035 MPa).

Temperature (°C)	S_u (MPa)
40	1034
100	1034
150	1034
200	1030
250	998
300	976
350	967
400	966
450	966
500	966
550	966
600	597
650	921
700	860
750	771
800	651
850	531
900	411

Table 8. Design values of tensile strength (S_u).

Rupture stress

The nominal values of rupture stress were calculated from a Larson-Miller model developed using data from [21]. A letter to DOE:EERE dated August 31st fully describes this model. Table 9 tabulates the nominal rupture stress vessels derived from the model.

		Time (hours)									
		1	10	30	100	300	1000	3000	10000	30000	100000
Temp. (°C)	425	9669	7466	6599	5765	5095	4451	3934	3437	3038	2654
	450	8053	6161	5422	4713	4147	3605	3173	2758	2427	2110
	475	6707	5084	4454	3853	3376	2920	2559	2214	1939	1678
	500	5586	4195	3659	3150	2748	2366	2064	1777	1550	1334
	525	4652	3462	3006	2576	2237	1916	1664	1426	1238	1061
	550	3875	2856	2470	2106	1821	1552	1342	1144	989	844
	575	3227	2357	2029	1722	1482	1257	1082	918	791	671
	600	2688	1945	1667	1407	1206	1019	873	737	632	533
	625	2238	1605	1369	1151	982	825	704	592	505	424
	650	1864	1324	1125	941	799	668	568	475	403	337
	675	1553	1093	924	769	650	541	458	381	322	268
	700	1293	902	759	629	529	439	369	306	257	213
	725	1077	744	624	514	431	355	298	245	206	170
	750	897	614	512	420	351	288	240	197	164	135
	775	747	507	421	344	286	233	194	158	131	107
	800	622	418	346	281	232	189	156	127	105	85
	825	518	345	284	230	189	153	126	102	84	68
	850	432	285	233	188	154	124	102	82	67	54
	875	359	235	192	154	125	100	82	66	54	43
	900	299	194	158	126	102	81	66	53	43	34

Table 9: Nominal rupture stresses.

The ASME Code uses a 95% prediction lower bound on the Larson-Miller models to derive allowable rupture stresses accounting for material variation. Table 10 tabulates values of rupture stress using this procedure.

		Time (hours)									
		1	10	30	100	300	1000	3000	10000	30000	100000
Temp. (°C)	425	8073	6283	5575	4890	4338	3804	3374	2958	2624	2300
	450	6762	5215	4607	4021	3552	3100	2737	2388	2109	1839
	475	5663	4328	3806	3306	2907	2525	2220	1927	1694	1470
	500	4743	3591	3144	2718	2380	2056	1800	1555	1360	1175
	525	3971	2979	2597	2234	1947	1674	1459	1254	1092	938
	550	3324	2471	2144	1836	1592	1363	1182	1011	876	749
	575	2783	2049	1770	1508	1302	1109	957	814	703	598
	600	2329	1699	1461	1238	1064	902	775	656	563	476
	625	1948	1408	1205	1016	870	733	627	528	451	380
	650	1630	1166	994	834	710	595	507	424	361	302
	675	1363	966	819	684	580	483	409	341	289	240
	700	1139	800	675	561	473	392	331	274	231	191
	725	952	662	556	459	386	318	267	220	184	152
	750	796	548	458	376	314	258	215	176	147	120
	775	665	453	377	308	256	209	173	141	117	96
	800	555	374	310	252	208	169	140	113	94	76
	825	463	309	255	206	169	137	112	91	74	60
	850	386	255	209	168	138	111	90	73	59	48
	875	322	211	172	137	112	89	73	58	47	38
	900	268	174	141	112	91	72	58	46	38	30

Table 10: Design rupture stresses (S_r) in MPa.

Section VIII allowable stress

The standard ASME Code allowable stresses are based on 100,000 hour rupture lives and time-independent strengths. Most of the values in the table are from the ASME 740H Code Case [20]. However, we extended the allowable stresses up to 900° C using our rupture stress correlation but scaling the results so that our values match the Code values at overlap temperature of 800° C.

Temperature (°C)	S_o (MPa)
40	295
100	295
150	295
200	279
250	276
300	276
350	276
400	276
450	276
500	276
550	276
600	274
650	226
700	146
750	84.1
800	34.5
850	21.8
900	13.8

Table 11. Allowable stress S_o.

Isochronous stress-strain curves

The development of isochronous stress-strain curves for 740H at 700° C and 750° C was described in a previous quarterly update. The equations used in the model are:

$$\varepsilon = \varepsilon_e + \varepsilon_p + \varepsilon_c$$

$$\varepsilon_e = \frac{\sigma}{E}$$

$$\varepsilon_p = \begin{cases} 0 & \sigma \le \sigma_p \\ \left(\frac{\sigma - \sigma_p}{k_1}\right)^{1/k_2} & \sigma > \sigma_p \end{cases}$$

$$\varepsilon_c = A\sigma^m t^n$$

and Table 12 lists the model constants. Figures 10 and 11 plot isochronous stress-strain curves for 700° C and 750° C.

Parameter	700° C	750° C
E	178000 MPa	173500 MPa
σ_p	418.7 MPa	402.1 MPa
k_1	2.4e2 MPa	2.4e2 MPa
k_2	0.289	0.289
A	9.53e-76	1.82e-60
m	25.7	20.4
n	2.92	3.37

Table 12. Material parameters for isochronous stress-strain curve model.

The lack of high temperature creep test data means we cannot determine isochronous curves for 800° C and 850° C. This is an important gap as it means we cannot evaluate strain limits above 750° C. For the present report if we required valued of the isochronous curves above 750° C we very crudely extrapolated from the 700° C and 750° C values.

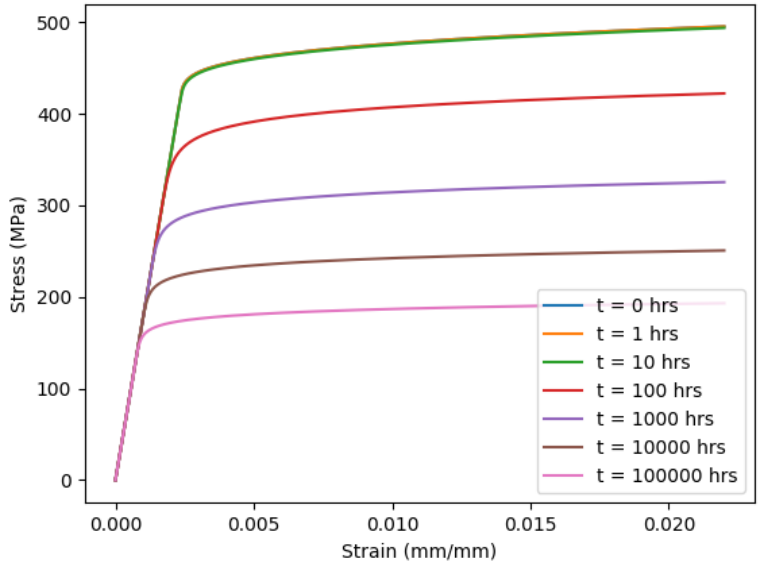

Figure 10: Isochronous stress-strain curves at 700° C.

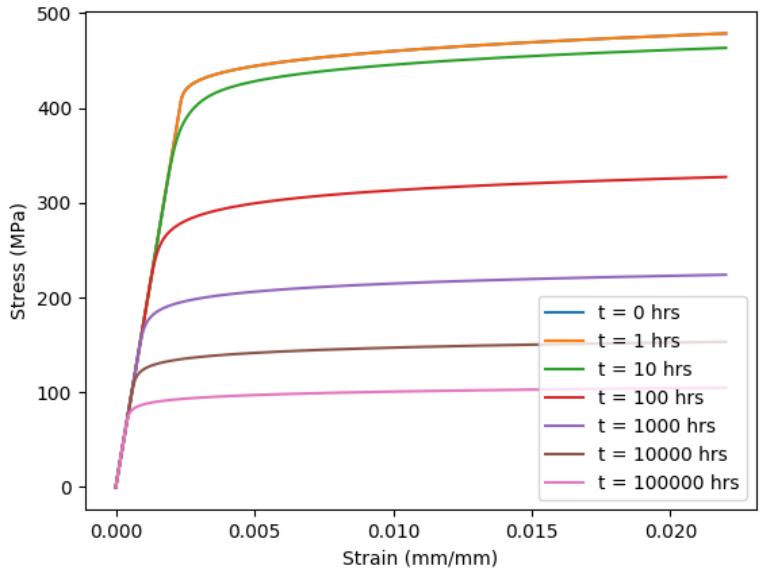

Figure 11: Isochronous stress-strain curves at 750° C.

Section III, Division 5 time dependent allowable stress

The Section III, Division 5 time-dependent allowable stress S_t is the lesser of 67% of the design rupture stress S_r, 80% of the stress required to produce tertiary creep, or 100% of the stress to cause 1% strain. Because we do not have complete isochronous curves, Table 13 shows values for this allowable based solely on the rupture criteria.

		Time (hours)									
		1	10	30	100	300	1000	3000	10000	30000	100000
Temp. (°C)	425	5382	4189	3717	3260	2892	2536	2249	1972	1749	1533
	450	4508	3477	3071	2681	2368	2066	1825	1592	1406	1226
	475	3776	2885	2538	2204	1938	1683	1480	1285	1129	980
	500	3162	2394	2096	1812	1586	1371	1200	1037	907	783
	525	2647	1986	1731	1489	1298	1116	972	836	728	626
	550	2216	1647	1430	1224	1062	908	788	674	584	499
	575	1855	1366	1180	1005	868	739	638	543	468	398
	600	1552	1132	974	825	710	601	516	437	375	318
	625	1299	939	803	677	580	489	418	352	301	253
	650	1087	778	663	556	473	397	338	283	241	201
	675	909	644	546	456	386	322	273	227	192	160
	700	476	475	450	374	315	262	220	183	154	127
	725	476	441	371	306	257	212	178	147	123	101
	750	461	365	305	251	209	172	143	118	98	80
	775	461	302	251	205	171	139	116	94	78	64
	800	370	249	207	168	139	113	93	76	62	51
	825	309	206	170	137	113	91	75	60	50	40
	850	257	170	139	112	92	74	60	48	40	32
	875	215	140	115	92	75	60	48	39	31	25
	900	179	116	94	75	61	48	39	31	25	20

Table 13: Time dependent allowable stress (S_t) in MPa.

Section III, Division 5 allowable stress

The Section III, Division 5 allowable stress S_{mt} is the lesser of the time dependent allowable stress S_t and 67% of the minimum specified yield stress, 33% of the minimum specified ultimate tensile stress, either 67% or 90% of the yield strength S_y, and 33% of the tensile strength S_u. For the yield strength which criteria is applied depends on the material's ductility. At least for this preliminary report we recommend using the 90% criteria as Alloy 740H has good room temperature ductility. Table 14 lists the values used in this update.

		Time (hours)									
		1	10	30	100	300	1000	3000	10000	30000	100000
Temp. (°C)	425	305	305	305	305	305	305	305	305	305	305
	450	302	302	302	302	302	302	302	302	302	302
	475	300	300	300	300	300	300	300	300	300	300
	500	297	297	297	297	297	297	297	297	297	297
	525	295	295	295	295	295	295	295	295	295	295
	550	293	293	293	293	293	293	293	293	293	293
	575	290	290	290	290	290	290	290	290	290	290
	600	288	288	288	288	288	288	288	288	288	288
	625	285	285	285	285	285	285	285	285	285	253
	650	283	283	283	283	283	283	283	283	241	201
	675	280	280	280	280	280	280	273	227	192	160
	700	278	278	278	278	278	262	220	183	154	127
	725	265	265	265	265	257	212	178	147	123	101
	750	248	248	248	248	209	172	143	118	98	80
	775	233	233	233	205	171	139	116	94	78	64
	800	210	210	207	168	139	113	93	76	62	51
	825	186	186	170	137	113	91	75	60	50	40
	850	163	163	139	112	92	74	60	48	40	32
	875	138	138	115	92	75	60	48	39	31	25
	900	133	116	94	75	61	48	39	31	25	20

Table 14: Section III, Division 5 allowable stress (S_{mt}) in MPa.

Fatigue curves

We were able to collect fatigue data for 740H for temperature in the 700° C to 800° C range [22-23]. Based on this data we constructed a nominal fatigue curve for high temperature use. To account for material variation, environmental effects, and other factors the Section III, Division 5 nuclear Code factors the nominal fatigue curve by a factor of 2 on strain range and 20 on the number of cycles to failure. Previous CSP design work has used factors of 1.5 and 10 respectively. Table 15 tabulates fatigue curves for nominal values, the nuclear factors, and the CSP factors. We will evaluate appropriate fatigue safety factors as part of our ongoing work. For now we are considering all three types of fatigue curves.

Cycles	Strain range, nominal (mm/mm)	Strain range, CSP (mm/mm)	Strain range, nuclear (mm/mm)
10	0.1280	0.0184	0.0143
20	0.0525	0.0143	0.0117
40	0.0300	0.0117	0.0100
100	0.0184	0.0096	0.0085
200	0.0143	0.0085	0.0071
400	0.0117	0.0076	0.0059
1000	0.0096	0.0064	0.0048
2000	0.0085	0.0056	0.0042
4000	0.0076	0.0051	0.0038
10000	0.0068	0.0045	0.0034
20000	0.0063	0.0042	0.0032
40000	0.0060	0.0040	0.0030
100000	0.0055	0.0037	0.0028
200000	0.0053	0.0035	0.0026
400000	0.0050	0.0034	0.0025
1000000	0.0048	0.0032	0.0024

Table 15. Fatigue curves used here for 740H at elevated temperatures.

Figure 12 plots the fatigue curves to provide a visual comparison.

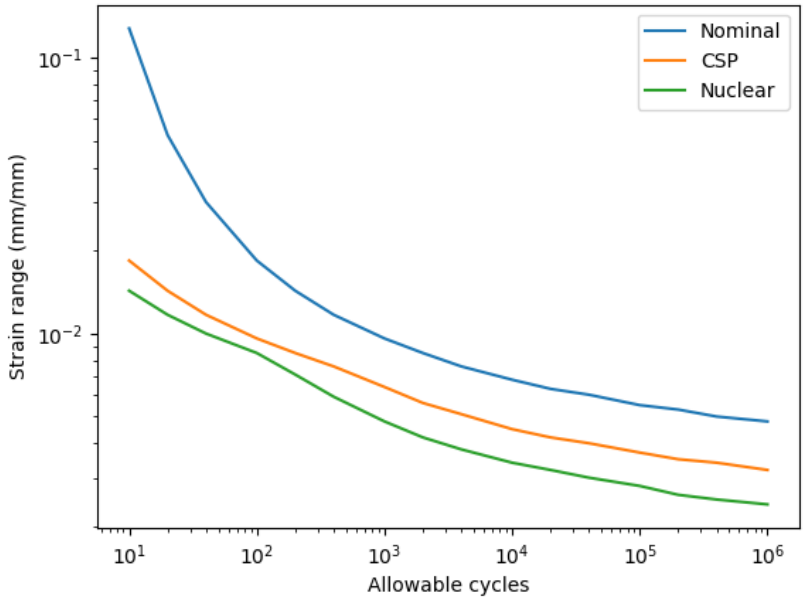

Figure 12. Nominal and design fatigue curves for different design factors.

Creep-fatigue interaction diagram

We have no creep-fatigue data to determine the creep-fatigue interaction diagram. For this preliminary design study we picked an intersection point of (0.1,0.1), the same diagram proposed for a similar nickel-based Alloy 617 for incorporation as a Section III, Division 5 high temperature material. We will need to wait for experimental data to validate this diagram, plotted as Figure 13.

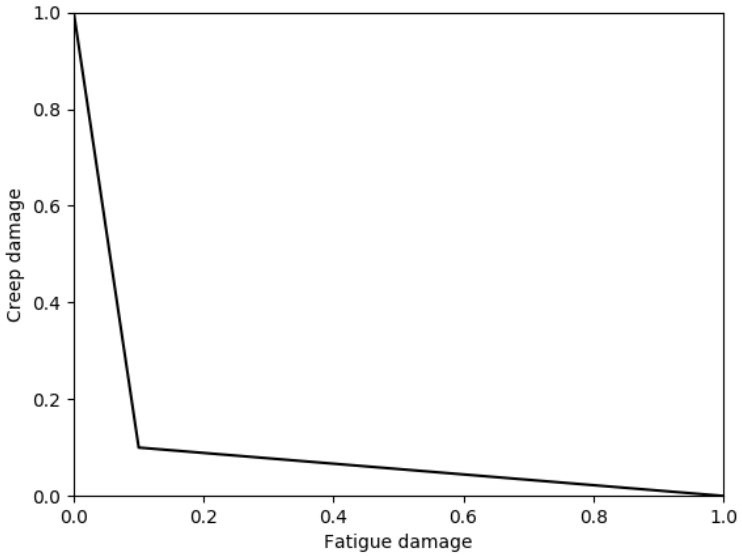

Figure 13. Creep fatigue-interaction diagram.

Notional inelastic model

Design by inelastic analysis requires an inelastic model that capture the relevant material deformation mechanisms. Assembling such a model is a substantial research project in its own right. However, for this trial analysis we created a very simple inelastic model that captures the gross features of the inelastic deformation of 740H.

The model has three contributions: elasticity, using the values of Young's modulus and Poisson's ratio described above, rate independent plasticity, and power law creep. The rate independent model is simple J_2 plasticity with a Voce hardening model calibrated to capture the manufacturer's yield, ultimate, and ductility data.

$$\sigma_{flow} = \sigma_0 + R\left(1 - e^{-\delta \varepsilon_p}\right)$$

Table 16 shows the constants for the elastic model, thermal model, and plastic Voce hardening model.

Temperature (°C)	E (MPa)	v	α	σ_0 (MPa)	R (MPa)	δ
25	221000	0.31	11.77	741	390	9.72
450	196500	0.31	15.53	657	336	9.88
500	193000	0.31	15.67	647	330	9.92
550	189500	0.31	16.16	638	323	9.92
600	186000	0.31	16.64	628	317	9.97
650	182000	0.31	17.75	618	310	9.97
700	178000	0.31	18.86	608	304	10.01
750	173500	0.31	20.49	560	255	10.23
800	169000	0.31	22.11	547	142	10.47
850	164500	0.31	24.25	521	14	10.56

Table 16. Elastic, thermal, and plastic properties for the inelastic model.

The power law creep prefactor and exponent are based on a physical scaling model developed. The model is setup to capture the experimental mean creep rate found in the available creep test data found in the literature [21,23] as a function of stress and temperature. The scalar creep model is

$$\dot{\varepsilon}_{cr} = \dot{\varepsilon}_0 e^{BF} \left(\frac{\sigma_{eq}}{\mu}\right)^{AF}$$

$$F = -\frac{\mu b^3}{kT}$$

Table 17 lists the creep model parameters in appropriate units. In this equation μ is the temperature-dependent shear modulus implied by the temperature dependent elastic modulus and constant Poisson's ratio in Table 16 and k is the Boltzmann constant.

Parameter	Value	Units
$\dot{\varepsilon}_0$	1.59e5	1/s
A	-0.182	-
B	-0.209	-
k	1.38064e-20	mJ/K
b	2.019e-7	mm

Table 17. Creep model parameters.

We only have a very limited set of data to work with so the model is used to extrapolate far beyond the experimental dataset and will likely be inaccurate at high temperatures.

Huddleston constant

To compute creep damage multiaxial stress states must be converted into an equivalent scalar stress measure. Section III, Division 5 uses the Huddleston model to make this conversion. This model requires determining a factor C which essentially quantifies the effect of stress triaxiality on creep damage.

In the absence of data, Huddleston's original paper recommends a value of $C = 0.24$ for austenitic materials. A single test at INL established a factor of $C = 0.25$ for A617, which is similar to 740H. Based on this data we will use a factor of $C = 0.25$.

Receiver model

This section describes a reference thermomechanical model of a tubular CSP receiver. The goal of this reference model is not to actually design a receiver, but rather to serve as a realistic test bed to assess different potential creep-fatigue and ratcheting design methods. As such, the goal is to be realistic but not to perfectly match any particular design details.

We considered an 8.5 m diameter, 10.5 m tall, 360° external cylindrical receivers as the reference model. Thermal and structural analysis of the receiver tubes were performed under the radiation heat flux map on the day of spring equinox. A computer code, called DELSOL3 [24], developed by Sandia National Laboratory was used to calculate the radiation heat flux map on the receiver. At first, an optimization calculation was run on DELSOL3 to determine the best combination of the tower height, receiver size, field layout, heliostat spacing, and tower position at electrical design power level of 45 MWe (and thermal power of 120 MWe) and flux limit of 1.2 MW/m^2. Once the system was optimized, the heat flux map on the receiver at different times of the day were determined. Figure 14 shows the radiation heat flux map at noon on the day of spring equinox for an optimal solar receiver system. 1D smart aiming at the centerline of the receiver was employed to determine the heat flux. As seen in the figure, radiation solar heat flux is maximum in the north hemisphere and minimum in the south hemisphere. As the heat flux is symmetric about north-south axis, two flow paths each containing 9 panels were considered. Salt enters the receiver at the north side through panel-1 and leaves the receiver at the south side from panel-9 (Figure 15). Each panel consists of 32 vertical tubes with 4.22 cm diameter and 1.65 mm thickness. The tube pitch was considered as 1.08 times the outer diameter.

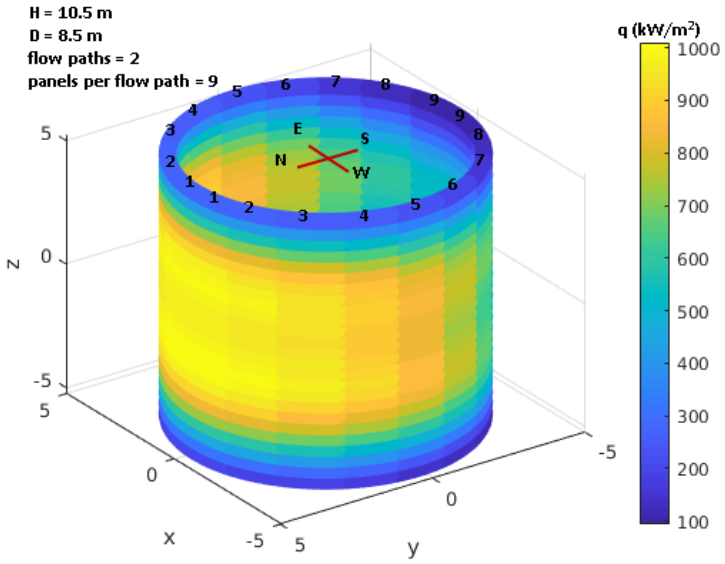

Figure 14: Heat flux distribution on the external receiver at noon on the day of spring equinox.

Thermal and structural analysis of the receiver tubes were performed in 3 steps. First, heat transfer analysis of the whole receiver was done by considering one tube per panel. A panel with maximum tube temperature was then selected for heat transfer analysis of all 32 tubes in that panel. In the last step, a coupled thermal-structural analysis was performed by considering 2 tubes at two extreme ends of that panel. Figure 15 shows all the FE models for thermal and structural analyses. During thermal simulation, half of the outer tube wall that faces heliostats was considered as heating surface as well as for convective and radiative heat loss to the environment, while the other half was considered as adiabatic surface. Circumferential distribution of the heat flux on the tube heating surface was employed using the cosine function (Figure 16a) [25]. For structural simulation of the 2 selected tubes, fixed displacement boundary condition was employed for bottom surface, while nodes on the top surface are fixed in x- and y-direction but can move equally in z-direction (Figure 16b). KCl-$MgCl_2$ eutectic molten salt with constant inlet and maximum outlet temperatures of 550°C and 720°C, respectively, was considered. Salt temperature was assumed to vary linearly along the flow path. Temperature dependent salt properties were used to determine temperature dependent convective heat transfer coefficient along the flow path. Figure 17 shows temperature dependent properties of KCl-$MgCl_2$ found in [26]. Temperature dependent properties, presented in Tables 3 to 7, were also used for the tube material (alloy 740H).

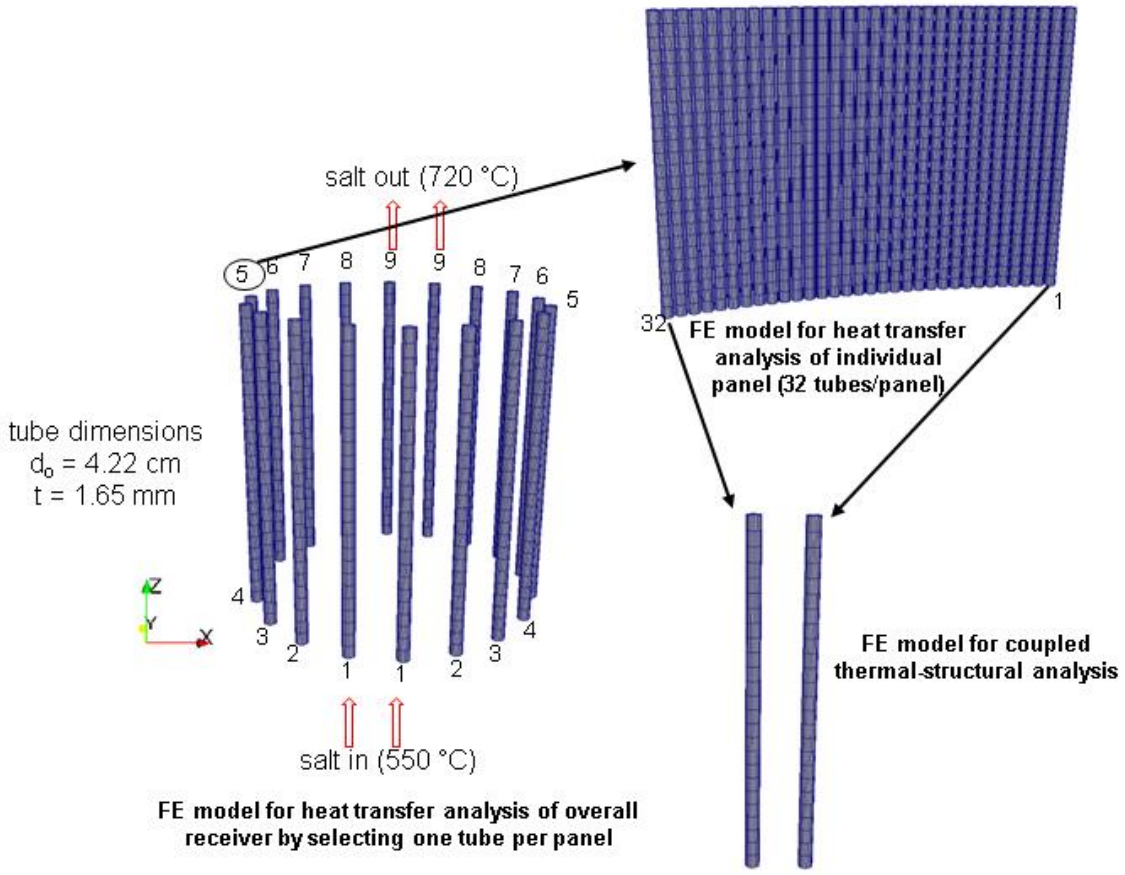

Figure 15. Finite element models for thermal and structural analysis of receiver tubes.

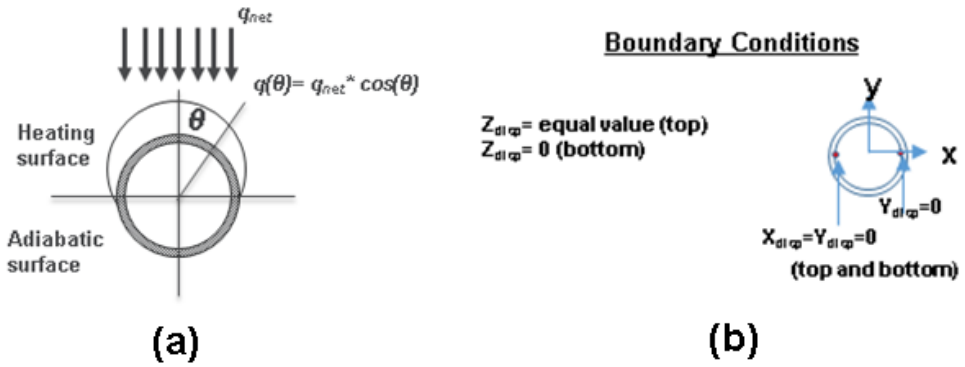

Figure 16. (a) Heat flux distribution scheme along the circumferential direction. (b) Displacement boundary conditions employed for structural simulation.

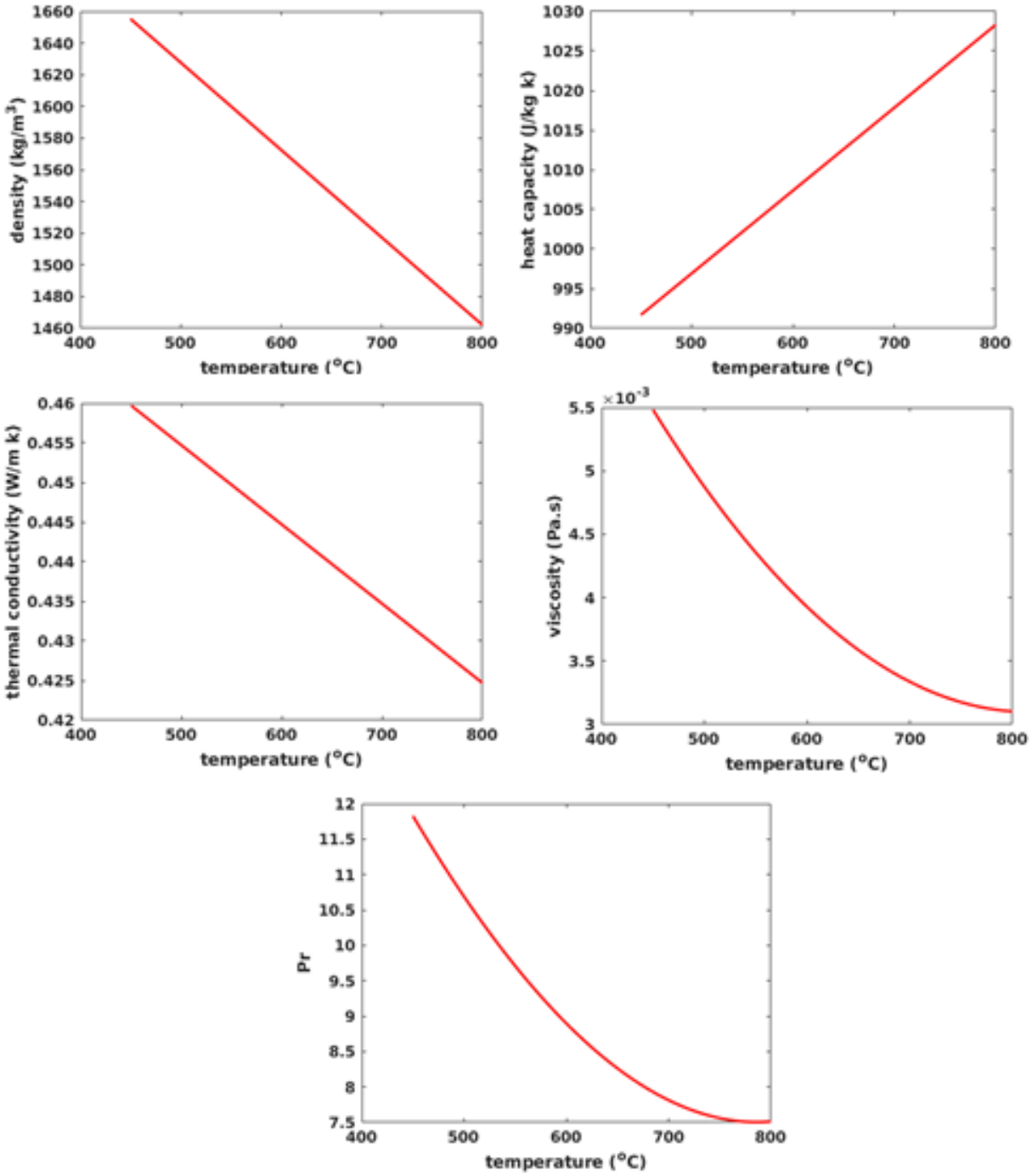

Figure 17. Temperature dependent properties of KCl-$MgCl_2$ salt.

Heat transfer analysis of the whole receiver was performed at several different salt mass flow rates. Figure 18 shows the evolution of outer wall temperature of the tubes in the whole receiver (considering one tube per panel) at different mass flow rates. The temperature contour plots are shown for radiation heat flux at noon on the day of spring equinox. Figure 18 also shows the total pressure drop between inlet and outlet, assuming tube surface roughness 0.05mm. At lowest mass flow rate, 286 kg/s, the

maximum tube wall temperature is found around 950 °C which is unfeasible. Increasing the flow rate to 572 kg/s reduces the maximum temperature to about 840 °C. Further increases in the mass flow rate of salt decrease the temperature of the tubes, however it comes at the cost of an increased pressure drop which requires higher salt pressure. As seen in Figure 18, although maximum tube temperature is decreased to 788 °C at 1430 kg/s flow rate, the pressure drop is increased to 5 MPa which is high for the tubes to pass primary load design at elevated temperature. We selected 572 kg/s as salt mass flow rate for thermal and structural analysis and design calculations of our receiver model. All the results shown in rest of the report are at 572kg/s salt mass flow rate.

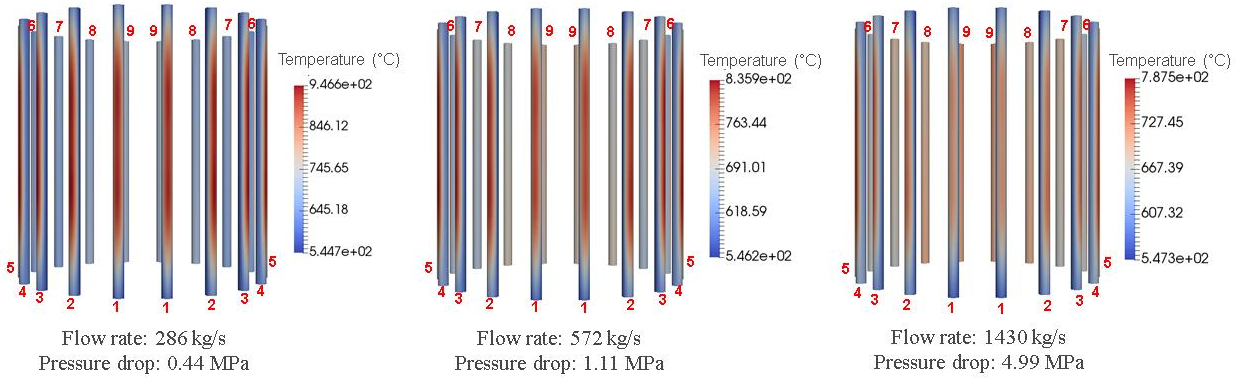

Figure 18. Outer wall temperature distribution at noon on the day of spring equinox and total pressure drop between inlet and outlet of the whole receiver at different salt mass flow rates.

From heat transfer analysis of the receiver model at 572 kg/s, tubes in panel-5 were found to be hotter than tubes in other panel and therefore panel-5 was considered for further thermal and structure analysis and design calculations. Figure 19 shows the temperature variation in outer surface of the tubes in panel-5. A comparison in maximum tube temperatures shows that tube 32 is the hottest while tube 1 is the coldest in panel-5. This is because tube 32 receives the highest radiation heat flux while tube 1 receives the lowest and the salt temperature profile does not vary among tubes with in a panel. Due to having two extreme temperature profiles, tubes 1 and 32 were considered for the coupled thermal-structural simulation. A better representation of the temperature variation across tube thickness and along the circumference can be seen in Figure 20 which shows the temperature contour plots of tube cross-sections at maximum through thickness averaged temperature for tubes 1 and 32. The two tube models are simulated for 100 hours- every 10 hours representing the radiation heat flux map for the whole day of spring equinox. Figure 21 compares the cyclic variation of maximum inner and outer wall temperatures for both the tubes. The difference in maximum temperature between outer wall and inner wall is around 60°C while it is 15°C between two tubes. The von Mises stress distribution at noon is shown in Figure 22. The figure also presents the cycle by cycle variation of the maximum von Mises stress for both tubes. The maximum von Mises stress in tube 32 is found to be 372 MPa while it is 332 MPa in tube 1. Figure 22 also shows the variation in von Mises stress across the thickness of the tube at an arbitrary location. Note that, structural simulation results

presented in this section are from inelastic analysis of the tubes by considering alloy 740H as an elastic-perfectly-plastic material which follows Norton-Bailey creep law. We used design values of yield strength (Sy), presented in Table 7, as yield stress for this analysis. However, for design calculations, presented in the following sections, inelastic analysis considering only elastic-perfectly-plastic material model with Code adjusted yield stress and elastic analysis of the tubes were performed.

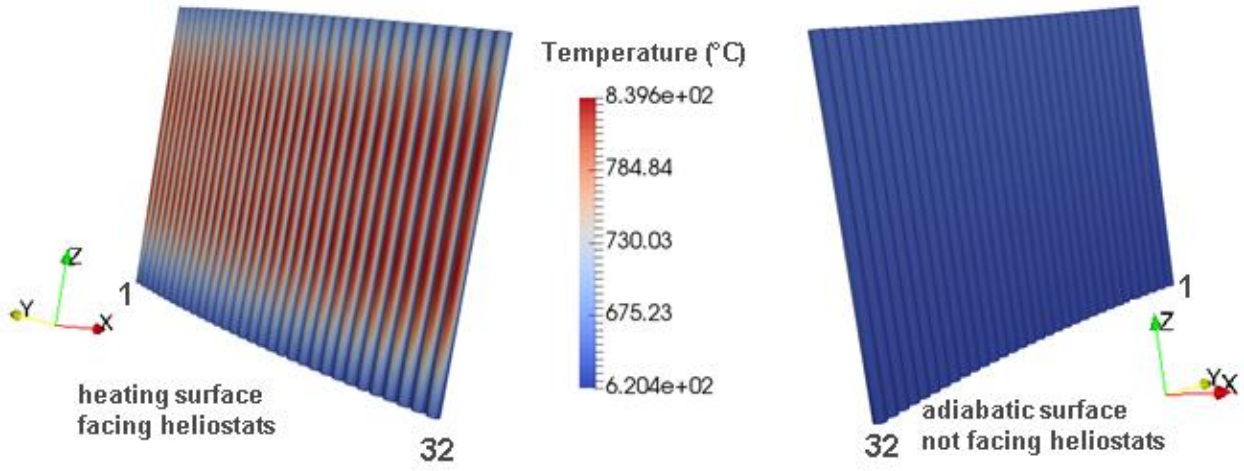

Figure 19. Outer wall temperature distribution in 32 tubes of panel-5 at noon on the day of spring equinox. (a) heating surface facing heliostats, (b) adiabatic surface not facing heliostats.

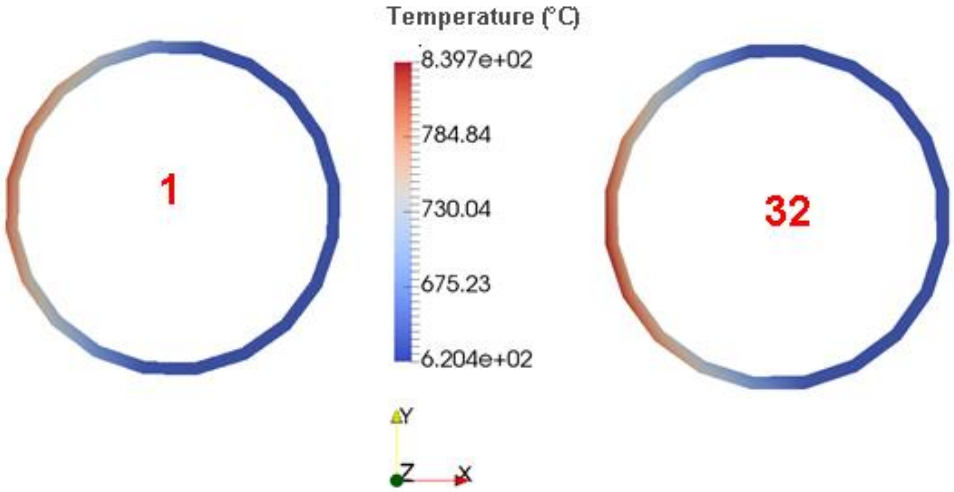

Figure 20. Radial and circumferential variation of temperature in tubes 1 and 32 of panel 9 at maximum through thickness averaged temperature locations at noon on the day of spring equinox.

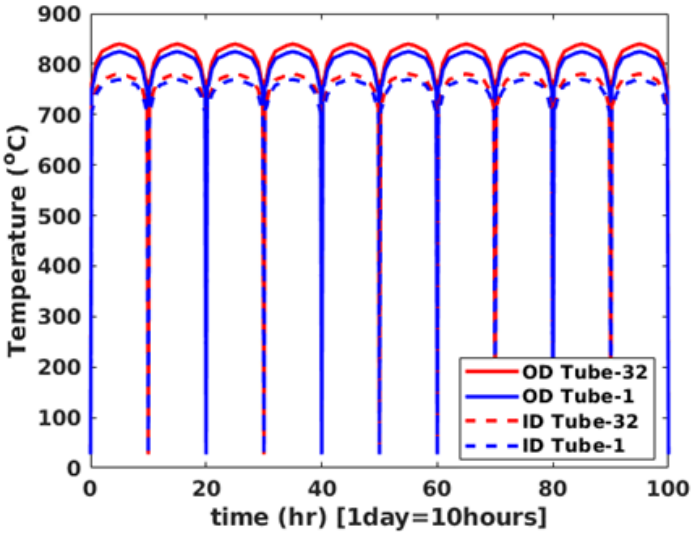

Figure 21. Maximum outer and inner wall temperatures in tubes 1 and 32 of panel-5 under spring equinox day heat flux cycles.

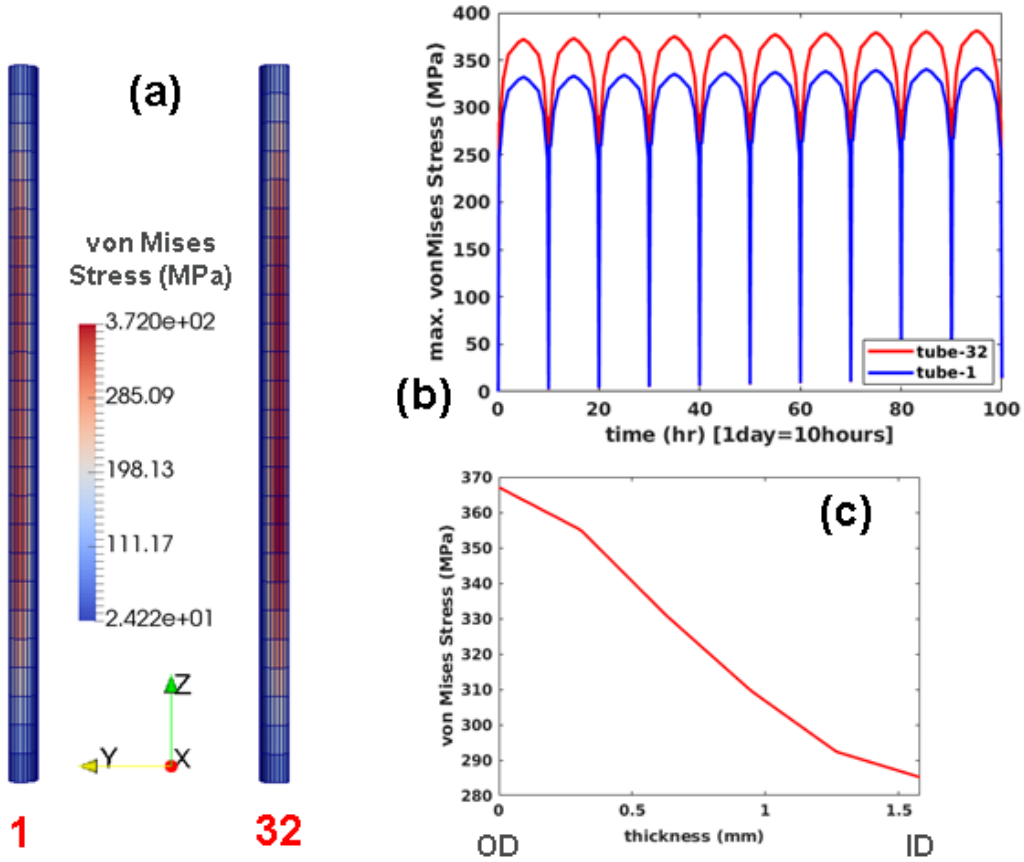

Figure 22. (a) Contour maps of the von Mises stress at noon on the day of spring equinox in tubes 1 and 32 of panel-5. (b) Maximum and minimum von Mises stress in tubes under spring equinox day heat flux cycles. (c) Von Mises stress plotted through the tube thickness at maximum wall averaged stress intensity location in tube 32.

Design methods

We evaluated the model receiver against three potential failure modes:

1. Primary load failure – the traditional ASME B&PV design by analysis method of evaluating structures for time independent plastic collapse and time dependent creep rupture.
2. Ratcheting – the time-dependent accumulation of excess strain, leading to service failures.
3. Creep-fatigue – the time-dependent accumulation of damage in the material leading to component failure.

Only the last two mechanisms are in the direct scope of the project. However, the traditional approach is to first check a structure against the primary load design criteria and then evaluate cyclic failure mechanisms, so we adhered to that conventional approach here.

We considered several different design methods based on Section VIII and Section III of the ASME Boiler & Pressure Vessel Code. For all these design methods we used the same set of underlying design data, described above.

Section VIII, Division 2 primary load design

Strictly, this section checks the receiver against the Section III, Division 5 S_o primary stress criteria. However, this check mimics the classical Section VIII, Division 2 design by analysis method and can be consider to represent commercial Section VIII practice. This check uses a design condition, which is the combination of the maximum pressure and temperature a receiver tube will see. Because this is a primary load check we can neglect the thermal stresses and calculate the primary membrane stress intensity with a simple analytic formula. The maximum receiver pressure is 2 MPa and the maximum metal temperature is approximately 840° C. The tube inner radius is 19.45 mm and the wall thickness is 1.65 mm. So the primary membrane stress intensity is

$$P_m = \sigma_{hoop} = \frac{pr}{t} = 23.6 \text{ MPa.}$$

The allowable stress intensity at 840° C is $S_o = 24.3$ MPa, which means the receiver passes this Code check.

There is no primary bending stress in the receiver so the bending design check is unnecessary.

Section III, Division 5 primary load design

The Section III, Division 5 primary load design check explicitly accounts for creep design life. The Code allows you to break up a single load cycle into multiple components and calculate the primary load using a life fraction summation. Figure 23 plots the wall averaged temperature at the critical tube location over a single load cycle.

The figure shows how we can divide the temperature history into a series of holds at constant temperature for computing the life fraction. The primary stress intensity is still 23.6 MPa.

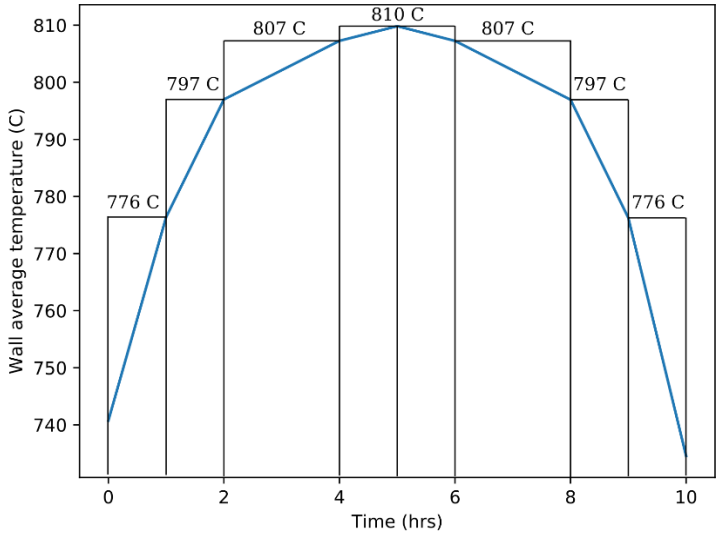

Figure 23: Discretized wall temperature history over a single cycle at the critical location in the receiver model.

The nuclear code requires classifying load cycle types and applies different design factors to different load types. Here we reasonably classify this operating load cycle as a Level A service load.

The life fraction sum determining the maximum component primary stress life is

$$n \sum_{i=1}^{n_{div}} \frac{t_i}{ti, allow} = 1$$

where t_i is the length of each subdivision in Figure 14 and $ti, allow$ is the allowable time, based on S_{mt}, for a stress intensity of 23.6 MPa at T_i, and n is the number of allowable load cycles, also equal to the receiver life in days.

Solving this equation gives a primary stress design life of about 20,000 days or 50 years.

Again, the primary bending load checks are not required here.

Section III, Division 5 ratcheting design by elastic analysis

We used the simplified inelastic analysis method described in HBB-T-1332 under Section III, Nonmandatory Appendix HBB-T of ASME BPVC [10] to determine the design life of receiver tubes based on creep ratcheting strain. This simplified inelastic analysis method uses primary and secondary stress intensity values computed using

elastic analysis. We classify the salt pressure as primary stress and thermal stress as secondary stress. Two separate finite element calculations were performed with temperature dependent elastic material model under only pressure loading and under only thermal loading to determine maximum primary stress intensity and maximum secondary stress intensity range, respectively. As tubes are straight, there is no bending stress component in primary loading. We considered a day – which is 10 hr of operational period on the day of spring equinox – as one cycle with maximum secondary stress intensity occurring at noon and minimum secondary stress intensity occurring at the beginning or end of the day when molten salt is completely removed from the receiver. Stress components from elastic analysis results were linearized through the wall of the tube and then were used to compute through thickness linearized Tresca stresses which were used to determine X and Y, as defined in HBB-T-1321(d) [10]. We used Test B-2 in HBB-T-1332 [10] to determine life of the tube based on ratcheting strain. Test B-2 uses X and Y to determine Effective Creep Stress parameter, Z using Figure HBB-T-1332-2 [10]. Z is used to determine Effective Creep Stress, σ_c. Design life is then determined by entering isochronous stress-strain curves at 1.25σc for 1% maximum creep ratcheting strain. We used the isochronous stress-strain plots at 750 °C (Figure 11) - the maximum temperature isochronous stress-strain plots are available – and extrapolated isochronous stress-strain plots at 840 °C – the maximum tube temperature to determine ratcheting strain based design life using elastic analysis method. The design life of the tube is found to be infinite and 255 cycles using isochronous curves at 750 °C and 840 °C, respectively.

Section III, Division 5 ratcheting design by elastic perfectly-plastic analysis

ASME BPVC Code Case – N861 [27] was used to determine design life of the receiver tube. Finite element calculation of the two tubes model was performed by considering the tube material as elastic-perfectly-plastic material and using temperature dependent pseudo-yield stress determined in accordance to Code Case – N861. Design life of the receiver tubes is found to be 5.08 cycles.

Section III, Division 5 ratcheting design by inelastic analysis

The Section III, Division 5 process for evaluating strain limits using inelastic analysis is essentially simply to run a full inelastic simulation, here using the model described above, and monitor the maximum principal (tensile) strain at the end of each cycle. The Code criteria are that the ratcheting strain does not exceed 1% average across a section or 5% at any point. Note this is essentially a service check using average material properties and no design factors. With this method the only decision to make for CSP components is determining the maximum allowable ratcheting strain.

Figure 24 plots the maximum principal strain at the critical tube location as a function of cycle count. The plot shows both the maximum strain across the cross-section and the average strain. The dashed lines were used to extrapolate the results out to the Code limits. The 1% mean criteria governed the design and the simulation reaches the criteria after 1963 days/cycles or 5.4 years.

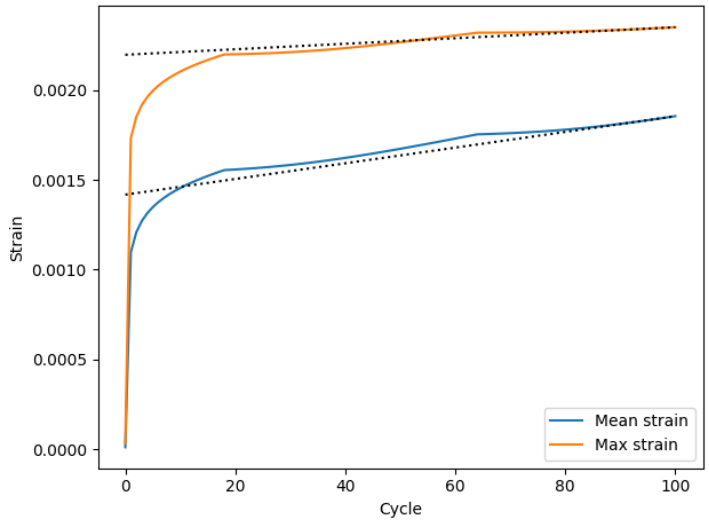

Figure 24. Ratcheting strain plotted as a function of cycle for the critical location in the receiver tube.

Section III, Division 5 creep-fatigue design by elastic analysis

According to HBB-T-1410 in Section III, Division 5 of ASME BPVC [25], a design is acceptable if the creep and fatigue damage satisfy the following relation:

$$\sum_j \left(\frac{n}{N_d}\right)_j + \sum_k \left(\frac{\Delta t}{T_d}\right)_k \leq D$$

where D is the total creep-fatigue damage and the first and second terms on the left side are fatigue damage and creep damage, respectively. In the fatigue damage term, $(n)_j$ is the number of repetitions of cycle type j and $(N_d)_j$ is the number of design allowable cycles for respective cycle type; while in the creep damage term, $(T_d)_k$ is the allowable time duration for a given stress at the maximum temperature occurring in the time interval k and $(\Delta t)_k$ is the duration of the time interval k.

The design allowable cycles for fatigue damage is determined by entering fatigue curves at strain range, ϵ_t. Strain range, ϵ_t is calculated using equation HBB-T-1432-16 [10]:

$$\epsilon_t = K_v \Delta\epsilon_{mod} + K\Delta\epsilon_c$$

where K is the local geometric concentration or equivalent stress concentration factor determined by dividing effective primary plus secondary plus peak stress divided by the effective primary plus secondary stress, K_v is the multiaxial plasticity and Poisson ratio adjustment factor, $\Delta\epsilon_c$ is the creep strain increment, and $\Delta\epsilon_{mod}$ is the modified maximum equivalent strain range.

$\Delta\epsilon_{mod}$ is the modified maximum equivalent strain range calculated using equation HBB-T-1432-12 [10]:

$$\Delta\epsilon_{mod} = (\frac{S^*}{\bar{S}})K^2\Delta\epsilon_{max}$$

where $\Delta\epsilon_{max}$ is calculated from the elastic analysis of tube under primary and secondary loading together. K is considered 1 as there is no peak stress in the loading considered for this study. In our future study, we plan to incorporate cloud events in heat flux profile which will eventually create peak stress in the receiver tubes. S^* and $\bar{S}$ are stresses determined by entering the isochronous stress-strain curves at $\Delta\epsilon_{max}$ and $K\Delta\epsilon_{max}$, respectively.

K_v is determined using equation HBB-T-1432-15 [25]:

$$K_v = 1.0 + f(K_v' - 1.0)$$

where f is the inelastic multiaxial adjustment factor determined using Figure HBB-T-1432-2 [10] and K_v' is the adjustment for inelastic biaxial Poisson's ratio determined from Figure HBB-T-1432-3 [10].

The creep strain increment per stress cycle, $\Delta\epsilon_c$ is determined by entering the isochronous stress-strain curves at 1.25σc for 10 hr (i.e. the period of each CSP loading cycle).

Once ϵ_t is computed, fatigue life of tubes is determined using fatigue curves shown in Figure 12. ϵ_t is found to be 0.26% and the corresponding allowable fatigue cycles are more than 1 million cycle using both Nominal and CSP design fatigue curves and 200,000 cycles using Nuclear design fatigue curve.

Creep damage evaluation from elastic analysis is done in accordance to HBB-T-1433(b). We used isochronous stress-strain curves at 750 °C (Figure 11) and at 840 °C (extrapolated) to determine the initial stress level values at those two temperatures. Entering Table 9 and 10 at the initial stress values as expected minimum stress-to-rupture, we determined the allowable time duration, T_d for the cases of nominal rupture stress and design rupture stress, respectively. The creep life is found to be 6.4 cycles and 2.8 cycles using nominal rupture and design rupture values, respectively, at 750 °C; while those are 0.96 cycles and 0.75 cycles, respectively, at 840 °C.

In summary, fatigue damage is negligible compared to creep damage and creep-fatigue life of tubes mostly depend on the creep damage accumulation. The calculated creep-fatigue life is shown in Table 18.

Fatigue properties / Creep properties	Nominal	CSP	Nuclear
750 °C, Nominal rupture stress	6.40	6.40	6.40
750 °C, Design rupture stress	2.80	2.80	2.80
840 °C, Nominal rupture stress	0.96	0.96	0.96
840 °C, Design rupture stress	0.75	0.75	0.75

Table 18. Creep-fatigue life (cycles) of receiver tubes determined using elastic analysis

Section III, Division 5 creep-fatigue design by elastic perfectly-plastic analysis

ASME BPVC Code Case – N862 [28] was used to determine design life of the receiver tube. Finite element calculation of the two tubes model was performed by considering the tube material as elastic-perfectly-plastic material and using temperature dependent pseudo-yield stress determined in accordance to Code Case – N862. Design life of the receiver tubes is found to be 0.4 and 0.12 cycles using nominal and design rupture stress, respectively.

Section III, Division 5 creep-fatigue design by inelastic analysis

Section III, Division 5 design by inelastic analysis starts from a full inelastic simulation using the model defined above. From this model we extract a representative strain range, using the Code definition, and a representative stress relaxation history. Thus far, these are average property calculations without design factors.

The representative strain range used here is 0.002708 mm/mm. The strain range is converted into an allowable number of cycles using the design fatigue curves. Here we have three options: nominal properties, the nuclear design factors of 2 on strain range and 20 on cycles and an intermediate case with a factor of 1.5 on strain range and 10 on cycles.

For creep damage first the stress tensor is converted into a scalar measure that accounts for the effect of triaxiality on creep rupture life. Section III, Division 5 uses the Huddleston model, which is well supported by experimental data. Figure 25 shows a representative stress-relaxation profile. Then, the scalar stress relaxation profile is converted into creep damage using the Code life-fraction rule. The Code specifies a minimum time to rupture, generally a 95% prediction bound on the data. This approach seems reasonable for CSP design as it simply accounts for batch-to-batch material variation. The Code applies an explicit design factor on this calculation of 0.67 for inelastic analysis and 0.9 for elastic analysis. Here we consider three options for CSP: factors of 0.67, 0.9, and 1.0.

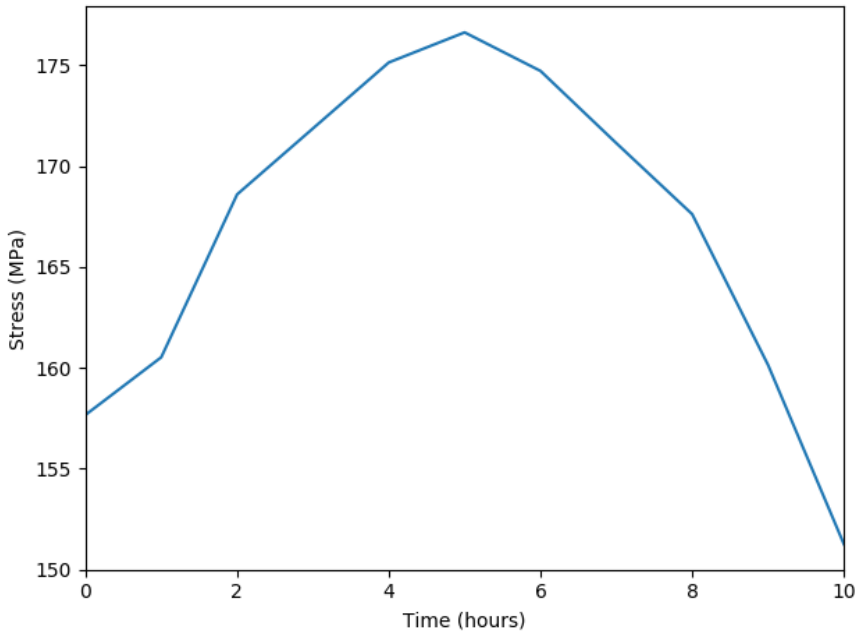

Figure 25. Huddleston effective stress relaxation profile used to calculate creep damage per cycle.

Finally, the creep and fatigue damages are compared to the creep-fatigue interaction diagram to determine if the design passes the creep-fatigue evaluation check. This diagram is based on nominal properties (though recall we do not have data to support a diagram specifically for 740H).

Table 19 summarizes the creep-fatigue design lives calculated using the options presented here.

		1.0 creep factor	0.9 creep factor	0.67 creep factor
Nuclear fatigue factors	D_c per cycle	0.000381	0.000719	0.004393
	D_f per cycle	6.85e-6	6.85e-6	6.85e-6
	Design life	2500 days	1333 days	171 days
CSP fatigue factors	D_c per cycle	0.000381	0.000719	0.004393
	D_f per cycle	~0.0	~0.0	~0.0
	Design life	2500 days	1333 days	171 days
Nominal fatigue	D_c per cycle	0.000381	0.000719	0.004393
	D_f per cycle	~0.0	~0.0	~0.0
	Design life	2500 days	1333 days	171 days

Table 19. Creep fatigue design lives using design by inelastic analysis for several different design factors.

Design method comparison and analysis

Ordering of methods based on conservatism

Though Section VIII design does not actually consider a real component lifetime the allowable stress is based on 100,000 hour rupture data (about 10 years). Taking this at face value, the Section III, Division 5 primary stress life of about 50 years is actually less conservative. The reason for this is that the Division 5 process takes into account the component's temperature and pressure history, rather than just considering a design load at the worst case combination of pressure and temperature. For design lives shorter than 10 years it may be worth developing a modified primary load design criteria for CSP systems.

Table 20 ranks the various ratcheting methods in order of conservatism. All three methods use nominal properties with no design factors. The only criteria to consider is the allowable ratcheting strain.

Method	Design life (cycles/days)
EPP	5
Elastic analysis	< 255
Inelastic analysis	1963

Table 20. Conservatism of various ratcheting design methods.

The general order is as expected. EPP is supposed to be simple to execute but very conservative and design by inelastic analysis is supposed to be less conservative, but difficult to execute, than design by elastic analysis.

Table 21 ranks the creep-fatigue design methods in order of conservatism.

Method	Design life (cycles/days)
EPP	< 1
Elastic analysis	1 to 3
Inelastic analysis (0.67 factor)	171
Inelastic analysis (0.9 factor)	1333

Table 21. Conservatism of various creep-fatigue design methods.

Again, the general ranking is as expected. The reference design is likely not suitable for creep-fatigue service and so all the design lives are very short. One item to address next quarter will be the 0.67 design factor applied to inelastic analysis in Section III, Division 5. This factor is much more severe than the general design factor of 0.9 used for elastic analysis. There is some historical justification for the more severe design factor, however we plan to reexamine this issue and reassess the required design factor for CSP systems.

Ordering of methods based on ease of use

For ease of use we can order the design methods on two axes: ease of analysis and ease of design calculations. Generally speaking, elastic analysis is the easiest, elastic perfectly-plastic somewhat harder, and inelastic analysis harder still. In terms of the design calculations, the methods rank in the opposite order: post processing inelastic

analysis is straightforward, EPP somewhat more complicated, and the elastic design rules are extremely complicated.

At first thought EPP would seem to be at a happy medium in between elastic and inelastic analysis. However, EPP has a severe disadvantage: though the required analysis is relatively straightforward it must be repeated multiple times in order to find the component's design life. In contrast for both elastic and inelastic analysis the analysis step must be performed only once and the design life can be computed from algebraic relations.

While inelastic analysis returns the least conservative and presumably most accurate design lives it is likely to be unpopular with CSP vendors. Inelastic analysis requires developing a sophisticated inelastic constitutive model describing the material behavior. This task is beyond the capabilities of most vendors and beyond the scope of the current project. Even assuming future DOE or industry sponsored research established a suitable inelastic model for 740H the required nonlinear transient analysis is still beyond common commercial practice. A design by inelastic analysis method requires the designer to follow all the expected load transients in their component for the entire component life. This requires an exceedingly lengthy computation for realistic components with multiple transients and this computation cannot be parallelized (as we have no available methods to parallelize simulations in time). In practice, this rules out inelastic analysis except for specialized design situations where a component redesign is impractical and a system designer has no choice but to spend the time required to complete an inelastic analysis.

Finally, all three design methods surveyed here do not easily adapt to FEA-based stress analysis. All three retain some of the ASME Code's historical focus on sections of vessels rather than single material points. This means some of the design calculations cannot be easily automated in a modern FEA workbench like ANSYS or Abaqus. EPP and inelastic analysis are much better than elastic analysis in this regard but both retain the ratcheting requirement referencing the average strain in a cross section.

Our tentative plan is to develop a creep-fatigue and ratcheting design method based on *simplified* inelastic analysis. This method will used history-independent elastic, perfectly-plastic, power law creep constitutive models to represent the stress and strain state in the component. Because this model does not depend on prior history, like a full inelastic constitutive model, cycles can be broken out and a designer does not need to simulate the full load history of their component. We will base the acceptance criteria on the criteria used for inelastic analysis in Section III, Division 5, reducing design factors where appropriate to reflect the lower consequences of failure in CSP systems. We will modify the Code acceptance criteria for ratcheting to reference only single material points, rather than sections, which will make the new method easy to implement in commercial FEA software. The acceptance criteria for creep-fatigue loading in Section III, Division 5 are already conceptually simple so we will adopt them with appropriate modifications.

Conclusions

Over the first three quarters of the project, the following has been accomplished:

1. Developed a thermomechanical model of a representative Gen 3 molten salt receiver.
2. Validated the model against other reference receiver designs and analysis results.
3. Down selected to Alloy 740H.
4. Procured Alloy 740H in plate and sheet forms.
5. Developed a trial set of design parameters for Alloy 740H using literature data.
6. Used these trial design parameters to evaluate several high temperature creep-fatigue and ratcheting design methods.
7. Recommended a modified version of Section III, Division 5 design by inelastic analysis for the CSP design method with simplified analysis and reduced design margin.
8. Performed 4 fatigue tests (750°C and 850°C).
9. Performed metallographic analysis on the tested fatigue specimens.
10. Met all proposed milestones.

Over the first three quarters of work, the candidate alloy for testing was selected, and initial testing begun. Additional, work was performed to develop a representative thermomechanical simulation of a tubular molten salt receiver using KCl-$MgCl_2$ eutectic molten salt with inlet and outlet temperatures of 550°C and 720°C respectively. A representative daily solar influxes using the DELSOL3 software [24] was established. These simulations provide a realistic testbed for evaluating creep-fatigue and ratcheting design methods.

One key result of these analysis is that the maximum metal temperature in the tubular receiver will be about 840°C. At this temperature our current design methods, using preliminary data, suggest a design governed by a creep-fatigue design life of about 3 years. This design life may be modified as the experimental data comes in, however, initial results suggest there is a large drop in material strength at these elevated temperatures. However, a decision will need to be made in collaboration with the program sponsors and CSP vendors to determine if a 3-year receiver life is viable. If not, the reference design may need to be modified to provide a realistic test system.

Budget and Schedule

Approximately $190,000 of the budget has been spent as of the end of this phase (10/31/18). This number does not include the purchase of the 740H material (Approximately $16,000). Task 1 is on track to ramp up testing, which will keep us on track for spending for the second year of the project.

Path Forward

Renewed work in the second year of the project (and work in Q4) will:

1. Finalize our recommendations for a design analysis method and provide the required analysis rules and guidelines.

2. Perform additional fatigue tests, as well as proposed creep-fatigue and creep tests.
3. Perform metallographic analysis necessary to understand failure of the tested specimens.
4. Perform similar tests on the sheet material form.
5. Provide final design parameters for Alloy 740H based on experimental data.
6. Determine appropriate creep-fatigue and ratcheting design margins and corresponding factors on the allowables.
7. Engauge with vendors to modify the proposed rules to incorporate their feedback.
8. Propose final design rules, summarized in the project final report.

Recommendations related to future work:

1. Unless less than five-year design lives are reasonable for receiver tubes alter the reference design to someone produce a lower maximum metal temperature and repeat these analyses. Guidance from DOE on this point is requested.
2. If design lives of less than 100,000 hours (about 10 years) are of interest include a modified primary load design methodology based on the Section III, Division 5 approach, with reduced design margin.
3. Develop short term isochronous curves for Alloy 740H up to the maximum metal temperature in the reference design.
4. Use experimental data, as it becomes available, to produce accurate design allowables are reevaluate the reference design as new information in included in the material property database.
5. *Tentative plan:* develop and propose creep-fatigue and ratcheting design rules based on simplified inelastic analysis.

References

[1] M. Mehos, C. Turchi et al., Concentrating Solar Power Gen3 Demonstration Roadmap NREL/TP-5500-67464 (2017).
[2] D.K. Fork, J. Fitch, S. Ziaei, R.I. Jetter, J. of Solar Energy Engin. 134 (2012).
[3] J. Ortega, S. Khivsara, J. Christian, C. Ho, P. Dutta, Applied Thermal Engin. 109 (2016) 979–987.
[4] Wait, David, "Development of 800°C Integrated Flow Channel Ceramic Receiver". United States. doi:10.2172/1460529. https://www.osti.gov/servlets/purl/1460529, 2018.
[5] P. Rodriguez, K.B.S. Rao, Prog. Mater. Sci. 37 (1993) 403-480.
[6] R. Hales, Fatigue of Eng. Mater. Struct. 3 (1980) 339-356.
[7] W.J. Plumbridge, E.G. Ellison, Mater. Sci. Technol. 3 (1987) 706-714.
[8] Special Metals website – www.specialmetals.com
[9] Haynes International website – www.haynesintl.com
[10] ASME, 2017, ASME Boiler and Pressure Vessel Code, Section III, ASME, New York.
[11] J.K. Wright, L.J. Carroll, et al., Proceedings of the ASME 2016 Pressure Vessels and Piping Conference PVP2016-63704 July 17-21, 2016, Vancouver, British Columbia, Canada.

[12] T.W. Neises, M.J. Wagner, A.K. Gray, Proceedings of the ASME 2014 8th Inter. Conference on Energy Sustainability ES2014 June 30-July 2, 2014, Boston, Massachusetts, USA.
[13] X. Chen, M.A. Sokolov, et al., Journal of Nuclear Materials 432 (2013) 94–101.
[14] L.J. Carroll, C. Cabet, M.C. Carroll, R.N. Wright, Inter. J. Fatigue, 47, 115-125 (2013).
[15] L. Carroll, INL/EXT-15-35132 Rev. 1, August 2015.
[16] J.M. Corum, J.J. Blass, PVP Pressure Vessel Piping Fatigue Fracture and Risk ASME 215 (1999) 147–153.
[17] T.C.Totemeier, CREEP8, 8th Inter. Conference on Creep and Fatigue at Elevated Temp., San Antonio, TX, July 22-26, 2007.
[18] P.G. Pritchard, L. Carroll, T. Hassan, Trans. of the Amer. Nuclear Soc., 109 (2013) 562-565.
[19] Special Metals,
http://www.specialmetals.com/assets/smc/documents/alloys/inconel/inconel-alloy-740-h.pdf.
[20] American Society of Mechanical Engineers Boiler & Pressure Vessel Code Case 2702, 2011.
[21] Purgert, R. et al. *Boiler materials for ultra supercritical coal power plants*. DOE technical report, 2015.
[22] Jena, P. S. M., et al. “Low cycle fatigue behavior of nickel base superalloy IN 740H at 760° C: Influence of fireside corrosion atmosphere.” *International Journal of Fatigue* 116: pp. 623-633, 2018.
[23] Zhang, S. and Takahashi, Y. “Evaluation of high temperature strength of a Ni-based Alloy 740H for advanced ultra-supercritical power plant.” In *Advances in Materials Technology for Fossil Power Plants: Proceedings from the Seventh International Conference*, Waikoloa, Hawaii, USA, 2014.
[24] Kistler, B. L. A user’s manual for DELSOL3: a computer code for calculating the optical performance and optimal system design for solar thermal central receiver plants. Sandia National Laboratories, Sandia Report No. SAND86-8018, 1986.
[25] Yang, X., et al. “Numerical simulation study on the heat transfer characteristics of the tube receiver of the solar thermal power tower.” *Applied Energy* 90, pp. 142-147, 2012.
[26] Xu, X., et al. “Experimental Test of Properties of KCl–MgCl2 Eutectic Molten Salt for Heat Transfer and Thermal Storage Fluid in Concentrated Solar Power Systems.*” Journal of Solar Energy Engineering* 140, pp. 051011, 2018.
[27] American Society of Mechanical Engineers Boiler & Pressure Vessel Code Case N-861, 2015.
[28] American Society of Mechanical Engineers Boiler & Pressure Vessel Code Case N-862, 2015.